



Stable *STIM1* Knockdown in Self-Renewing Human Neural Precursors Promotes Premature Neural Differentiation

Renjitha Gopurappilly, Bipan Kumar Deb, Pragnya Chakraborty and Gaiti Hasan*

National Centre for Biological Sciences, Tata Institute of Fundamental Research, Bengaluru, India

OPEN ACCESS

Edited by:

Daniel F. Gilbert,
Friedrich-Alexander-Universität
Erlangen-Nürnberg, Germany

Reviewed by:

Stefan Hauser,
Deutsches Zentrum für
Neurodegenerative Erkrankungen
(DZNE), Germany
Michael Chvanov,
University of Liverpool,
United Kingdom
Hyunsoo Shawn J. E.,
National University of Singapore,
Singapore
Philip Forsyth Copenhaver,
Oregon Health & Science University,
United States

*Correspondence:

Gaiti Hasan
gaiti@ncbs.res.in

Received: 27 January 2018

Accepted: 09 May 2018

Published: 11 June 2018

Citation:

Gopurappilly R, Deb BK,
Chakraborty P and Hasan G (2018)
Stable *STIM1* Knockdown
in Self-Renewing Human Neural
Precursors Promotes Premature
Neural Differentiation.
Front. Mol. Neurosci. 11:178.
doi: 10.3389/fnmol.2018.00178

Ca²⁺ signaling plays a significant role in the development of the vertebrate nervous system where it regulates neurite growth as well as synapse and neurotransmitter specification. Elucidating the role of Ca²⁺ signaling in mammalian neuronal development has been largely restricted to either small animal models or primary cultures. Here we derived human neural precursor cells (NPCs) from human embryonic stem cells to understand the functional significance of a less understood arm of calcium signaling, Store-operated Ca²⁺ entry or SOCE, in neuronal development. Human NPCs exhibited robust SOCE, which was significantly attenuated by expression of a stable shRNA-miR targeted toward the SOCE molecule, *STIM1*. Along with the plasma membrane channel Orai, *STIM1* is an essential component of SOCE in many cell types, where it regulates gene expression. Therefore, we measured global gene expression in human NPCs with and without *STIM1* knockdown. Interestingly, pathways down-regulated through *STIM1* knockdown were related to cell proliferation and DNA replication processes, whereas post-synaptic signaling was identified as an up-regulated process. To understand the functional significance of these gene expression changes we measured the self-renewal capacity of NPCs with *STIM1* knockdown. The *STIM1* knockdown NPCs demonstrated significantly reduced neurosphere size and number as well as precocious spontaneous differentiation toward the neuronal lineage, as compared to control cells. These findings demonstrate that *STIM1* mediated SOCE in human NPCs regulates gene expression changes, that *in vivo* are likely to physiologically modulate the self-renewal and differentiation of NPCs.

Keywords: calcium signaling, SOCE, inducible shRNA-miR, RNA-Seq, neural development

INTRODUCTION

The advent of pluripotent stem cells in the past decade, which includes embryonic stem cells (ESC) and induced pluripotent stem cells (iPSCs) and their neural derivatives, has allowed direct cellular and molecular analysis of human cell-derived brain progenitors as well as differentiated neurons. This is in contrast to earlier studies where understanding the biology and function of

human brain cells was largely restricted to post-mortem and pathological specimens (Di Lullo and Kriegstein, 2017). From cellular studies in other organisms it is evident that Ca^{2+} signaling affects a range of neural activities during development including neurotransmitter specification (Marek et al., 2010; Spitzer, 2012; Plazas et al., 2013; Guemez-Gamboa et al., 2014), synaptogenesis and neurite extension (Rusanescu et al., 1995; Rosenberg and Spitzer, 2011; Kawamoto et al., 2012). Besides well-documented modes of Ca^{2+} entry in neuronal cells through ligand and voltage-gated Ca^{2+} channels, it is evident that Endoplasmic Reticulum-driven store-operated Ca^{2+} entry (SOCE), also functions in neurons (Bardo et al., 2006). Store-operated Ca^{2+} entry (SOCE) is based on the interaction of STIM proteins, that sense Ca^{2+} levels in the Endoplasmic Reticulum (ER; Liou et al., 2005; Roos et al., 2005), with the Orai Ca^{2+} channel in the plasma membrane and was first described in non-excitable cells (Feske et al., 2006; Vig et al., 2006; Zhang et al., 2006). More recently it has also been characterized in excitable cells (Venkiteswaran and Hasan, 2009; Hartmann et al., 2014; Lalonde et al., 2014; Pathak et al., 2015) where significant roles for intracellular Ca^{2+} stores, and potentially SOCE, have been suggested in neurogenesis and neural development (Toth et al., 2016). Neuronal SOCE has been recognized as an important mechanism that neurons use to replenish Ca^{2+} stores during cell activation. As in non-excitable cells, SOCE might also initiate specific signaling pathways in NPCs and differentiated neurons (Majewski and Kuznicki, 2015).

SOCE through Orai channels has been investigated in mouse NPCs, isolated from embryos where it regulates gene transcription through calcineurin/NFAT (nuclear factor of T cells) signaling (Somasundaram et al., 2014). Interestingly, the attenuation of SOCE in mouse NPCs reduced their proliferation *in vitro*, as well as in the sub-ventricular zone (SVZ) of adult mouse brains *in vivo* (Somasundaram et al., 2014). Moreover, a recent study demonstrated that pharmacological blockade of SOCE in mouse SVZ neural stem cells decreased proliferation and impaired self-renewal by shifting the type of SVZ stem cell division from symmetric proliferative to asymmetric (Domenichini et al., 2018). Although mechanisms of neurogenesis are largely conserved among mammals, human neurogenesis shows some distinct attributes when compared to that of rodents, such as the presence of an astrocyte ribbon in the sub-ventricular zone (SVZ), higher turnover of hippocampal neurons and a rapid decline in the rate of neurogenesis with age (Sanai et al., 2004; Knoth et al., 2010; Wang et al., 2011). In the adult rodent brain NSCs continue to give rise to new neurons (van Praag et al., 2002; Toni et al., 2008), whereas adult neurogenesis in humans is still controversial (Boldrini et al., 2018; Sorrells et al., 2018). Rates of cell growth and neural lineage differentiation between primary rodent and human NSCs/NPCs are also reported to be dissimilar (Ostenfeld et al., 2002). Human stem cell-derived NPCs exhibit greater variation in neurite outgrowths when compared to rat cortical cultures (Harrill et al., 2011). *In vitro*, human NPC lines and mouse-derived cell lines respond differently to multiple stimuli, including *trans*-retinoic acid known to affect proliferation and induce apoptosis (Culbreth et al., 2012).

Furthermore, differences in cell surface markers (Klassen et al., 2001) and shorter telomeres have been demonstrated in hNPCs (Ostenfeld et al., 2000) as compared to their rodent counterparts. Independent studies in human neural precursors and differentiated neurons are thus essential to understand how STIM/Orai based SOCE might impact human brain development and function.

To understand the functional significance of SOCE-regulated gene expression in human neural cell specification we generated human NPCs (hNPCs) from a human embryonic stem cell line. The hNPCs exhibit robust SOCE that was significantly attenuated by knockdown of *STIM1*. Global transcriptomic analysis of *STIM1* knockdown hNPCs revealed downregulation of pathways associated with cell proliferation and concomitantly an upregulation of genes for neural differentiation. These changes in gene expression correlate with reduced proliferation and early neural differentiation in *STIM1* knockdown hNPC cultures indicating that the loss of SOCE *in vivo* could result in cessation of sufficient hNPCs, required for normal brain development.

MATERIALS AND METHODS

Experimental Design

We hypothesized that abrogating store-operated Ca^{2+} entry (SOCE), the less studied arm of endoplasmic reticular (ER) centric Ca^{2+} homeostasis mechanisms, in human neural precursors (hNPCs), may lead to disruption of their normal function based on studies of various neuronal cell types in rodents (reviewed by Toth et al., 2016) and *Drosophila* (Pathak et al., 2015, 2017; Richhariya et al., 2017). We generated small molecule induced hNPCs from a well-characterized human embryonic stem cell line (hESCs) (Reinhardt et al., 2013) and successfully knocked down *STIM1*, an essential element of SOCE, through lentiviral transduction to obtain expandable stable *STIM1* knockdown hNPC lines. Ca^{2+} imaging and immunoblots confirmed *STIM1* knockdown and the attenuation of SOCE. To investigate cellular and molecular changes brought about by loss of SOCE RNAseq analyses of the *STIM1* knockdown NPCs and their appropriate vector controls were performed that helped to identify significant changes in gene expression. Changes in expression levels of selected genes, identified by RNAseq, were further validated by real-time PCR. To understand the functional significance of SOCE-regulated changes in gene expression, Gene Ontology analyses were performed and a set of enriched biological pathways were identified that underwent significant up or downregulation. The identified pathways helped design experiments for phenotypic and functional characterization of the *STIM1* knockdown NPCs. Such experiments based on the identified GO pathways, corroborated a cell fate change in *STIM1* knockdown NPCs (**Supplementary Figure S1**). Details of the bioinformatics analyses, statistical tests performed and methods for the wet lab experiments are provided in the following segments.

Maintenance and Neural Induction of Human Embryonic Stem Cells (hESCs)

All experiments, performed with hESC lines, were approved by the Institutional Committee for Stem Cell Research, registered under the National Apex Committee for Stem Cell Research and Therapy, Indian Council of Medical Research, Ministry of Health, New Delhi. The hESC cell line H9/WA09 (RRID: CVCL_9773) was used for this study. Undifferentiated hESCs were initially cultured on irradiated mouse embryonic fibroblasts and gradually adapted to grow under feeder-free conditions by culturing on 0.5% Matrigel in complete mTeSR media (Stem Cell Technologies, Vancouver, BC, Canada). Passage of cells was initiated by washing with phosphate-buffered saline (PBS) followed by incubation at 37°C in CTK dissociation solution (PBS with 0.25% trypsin, 1 mg/mL collagenase IV, 20% KSR, all from Invitrogen, Carlsbad, CA, United States and 1 mM CaCl₂ from Sigma, St Louis, MO, United States). hESC cultures were allowed to form embryoid bodies (EBs) by forced aggregation in low attachment dishes. For neural induction, as described earlier (Reinhardt et al., 2013; Louis et al., 2017) 2-day EBs, were supplemented with 10 mM SB431542 (Stem Cell Technologies), 1 mM dorsomorphin (Tocris Cookson, Ballwin, MO, United States), 3 mM CHIR99021 (Stem Cell Technologies) and 0.5 mM purmorphamine in suspension cultures. Four-day EBs were treated with 1:1 DMEM/F12 neurobasal medium supplemented with 1:200 N2, 1:100 B27 along with neural induction media factors in suspension cultures. Six-day old EBs were plated onto Matrigel-coated plates in maintenance medium containing 1:1 DMEM/F12 neurobasal medium supplemented with 1:200 N2, 1:100 B27, 3 μM CHIR99021, 0.5 mM purmorphamine and 150 μM ascorbic acid (Sigma, St Louis, MO, United States). Neural precursor cells (NPCs) were then passaged enzymatically with Accutase (Invitrogen) and stored frozen in liquid nitrogen. Batches of frozen NPCs were thawed and plated as per requirement (protocol adapted from Reinhardt et al., 2013). NPCs could be maintained for >25 passages, though for all experiments described here we used cells from passage numbers of less than 25. For spontaneous differentiation, neural precursors were allowed to grow in media, without small molecules and in the presence of N2 and B27 supplements, for 14–21 days. Media was replenished every alternate day for NPCs and for spontaneously differentiating cultures.

shRNA-miRs and Lentiviral Transduction for *STIM1* Knockdown

ShERWOOD-UltramiR short hairpin RNA (shRNA), are vector-based RNAi triggers with a new generation shRNA-specific design and an optimized microRNA scaffold “UltramiR” (Auyeung et al., 2013; Knott et al., 2014). *STIM1* knock-down was performed using a mixture of *STIM1*- ULTRA-3374033 (TAATATTGCACCTCCACCTCAT), ULTRA-3374029 (TTTATGATCTACATCATCCAGG) and ULTRA-3374031 (TCCAGTGAGTGGATGCCAGGGT) (transOMIC Technologies, Huntsville) in NPCs. A Non-Targeting shRNA Construct (NTC) was used as a control for all experiments. The inducible ZIP

(all-in-one) vector contains the components necessary for regulated expression of the shRNA-mir, including the TRE3GS inducible promoter positioned upstream of the shRNA, and the Tet-On 3G transcriptional activator (Tet-On 3G TA), which is expressed constitutively from an internal promoter. The Tet-On 3G TA binds to the TRE3GS promoter in the presence of doxycycline and induces expression of ZsGreen and the shRNA-mir. This allows for direct visual confirmation of induced shRNA expression. A puromycin resistance gene (PuroR) is also encoded for rapid selection of transduced cells. The lentiviral transfer vector (pZIP) was co-transfected with the desired packaging vectors (pCMV-dR8.2 and pCMV-VSVG from Addgene RRID: SCR_002037) encoding the *env*, *gag* and *pol* protein into a packaging cell line (HEK293T-ATCC Cat# CRL-3216, RRID: CVCL_0063). The transfer vector contained sequences that package as the viral genome. The sequences encode an shRNA-mir against *STIM1* and a selection cassette, both of which integrate into the target cell's genome. Viral particles, released from the packaging cell, were harvested from the supernatant for 3 days as follows. Virus-containing supernatant was filtered through 0.45 μm PVDF syringe filters (Millipore), concentrated using a Lenti-X-concentrator, tested with Lenti-X GoStix (Clontech) and applied to NPCs (P-10) at an MOI of 10. After 24 hrs the media surrounding the NPCs was discarded and fresh media with doxycycline was added to induce shRNA expression. Cells were maintained in doxycycline containing media for a minimum of 5 passages to obtain an NPC cell line with stable knockdown. Cell counts and growth curves of the NTC and *STIM1* KD cells were obtained by the Trypan Blue exclusion method. The MTT [3-(4,5-dimethylthiazol-2-yl)-2,5-diphenyltetrazolium bromide, Sigma] assay for proliferation was performed as described earlier (Burke and Kukoly, 2008).

Ca²⁺-Imaging in hNPCs

Ca²⁺-measurements were performed on hNPCs plated as single cells on poly-D-lysine (PDL) coated coverslips. After plating, cells were allowed to attach for 24 h prior to imaging. Cells were washed thrice with the culture medium, following which they were loaded with 5 μM of the ratiometric Ca²⁺-indicator Indo-1 acetoxymethylester (AM, Invitrogen,) which was dissolved in the culture medium and supplemented with 0.002% Pluronic F-127 in dark for 45 min. Following this, the cells were washed three times with the culture medium and kept in it until imaging. Just before the start of imaging, the culture medium was replaced with ‘0 Ca²⁺ HBSS’ (20 mM HEPES, 137 mM NaCl, 5 mM KCl, 2 mM MgCl₂, pH = 7.3) supplemented with 0.5 mM EGTA and 10 mM Glucose. To check for inhibition of SOCE, inhibitors of the SOC-channel, BTP-2 (Invitrogen) and 2-APB (Invitrogen) or DMSO (solvent control) were dissolved in the indicated concentration in 100 μl of the ‘0 Ca²⁺ HBSS.’ For these experiments, the culture medium in which the cells were kept after washing was replaced by HBSS containing either the inhibitors or DMSO and imaged. Therefore, the SOCE-inhibitors were present in the external medium throughout the course of the imaging. Ca²⁺ changes

were recorded from single cells using a 60X oil objective (NA = 1.35) and 350-nm excitation and 405/485 dual-emission filter sets in an Olympus IX81-ZDC2 Focus Drift Compensating Inverted Microscope. Basal changes in cytosolic Ca^{2+} in '0 Ca^{2+} HBSS' were recorded every 5s for 10 frames, after which Thapsigargin (TG, 10 μM , Invitrogen) was added to the cells to induce ER store Ca^{2+} release. After acquiring cytosolic Ca^{2+} changes every 15 s for 30 frames, 2 mM CaCl_2 was added to the cells to induce SOCE, which was also recorded every 15 s for 30 frames. 10 μM Ionomycin (Calbiochem) was finally added to record the maximum fluorescence values obtained after saturating the dye with Ca^{2+} . Image acquisition was performed using the Andor iXON 897E EMCCD camera and AndoriQ 2.4.2 imaging software (RRID: SCR_014461). The time-lapse acquisition mode of the software was used to follow fluorescence changes over time. A region of interest (ROI) was drawn manually around each cell. Fluorescence intensities of single cells were computed with ImageJ (RRID: SCR_003070) at 405 and 485 nm and these were used to calculate the F405/485 ratio for each time point. The F405/485 indicates the ratio of the fluorescence intensity emitted by the ' Ca^{2+} -bound' to the ' Ca^{2+} -unbound' form of the dye in the cells at each time point. Ca^{2+} responses from several cells were averaged and the mean (\pm SEM) across different time points was used to represent Ca^{2+} -responses during store-release and SOCE. Peak F405/485 values were quantified as box-plots, where the box represents the spread between 25 and 75% of the data, using Origin 8.0 software (RRID: SCR_014212). Horizontal lines in the center of the box represent the median and the smaller squares represent the mean. Statistical significance was computed among data sets using Mann-Whitney *U* test after applying the Bonferroni correction. Unless otherwise mentioned, all chemicals were obtained from Sigma.

Quantification of basal cytosolic $[\text{Ca}^{2+}]$ from hNPCs was performed using the dual-excitation single emission ratiometric Ca^{2+} -indicator Fura-2-AM. hNPCs plated as single adherent cells on PDL-coated coverslips were washed thrice with culture medium, following which they were loaded with 5 μM Fura-2-AM, in the dark, for 45 min at room temperature. The dye was dissolved in culture medium supplemented with 0.002% Pluronic F-127. After dye loading, cells were washed thrice with culture medium. The culture medium was finally replaced with HBSS containing 2 mM Ca^{2+} (20 mM HEPES, 137 mM NaCl, 5 mM KCl, 10 mM Glucose, 1 mM MgCl_2 , 2 mM CaCl_2 , pH = 7.3). Fura-2 was excited using dual 340/380 nm excitation and the emission intensity was recorded at 510 nm. Basal changes in cytosolic Ca^{2+} were recorded for 10 frames at an interval of 5 s. To obtain the minimum fluorescence values, 10 mM EGTA was added for chelating all available cytosolic Ca^{2+} , following which fluorescence changes were recorded every 5 s for 85 frames. Subsequently, the extracellular medium was supplemented with 10 mM Ca^{2+} . The maximum fluorescence intensities were recorded after saturating the dye loaded within the cell with Ca^{2+} , by adding 10 μM Ionomycin. Images were acquired after Ionomycin addition for 20 frames at 5 s interval. The peak fluorescence value was generally

obtained within the first 2 frames (corresponding to 10 s) of Ionomycin addition. Emission intensities corresponding to excitation at 340 and 380 nm were used to calculate the F340/380 ratio for each cell across all time points. The basal F340/380 at the start of imaging ($t = 0$) was calibrated to $[\text{Ca}^{2+}]$ using the Grynkiewicz equation (Grynkiewicz et al., 1985) as follows:

$$[\text{Ca}^{2+}](\text{nM}) = K_d \times \beta \times (R - R_{\min}) / (R_{\max} - R),$$

where R_{\min} and R_{\max} correspond to the minimum F340/380 and maximum F340/380 obtained after EGTA and Ionomycin addition, respectively. K_d for Fura-2 in human cells was taken as ~ 225 nM (Forostyak et al., 2013) and the scaling factor $\beta = 5$, was based on the ratio of the fluorescence emission intensities of Ca^{2+} -free and Ca^{2+} -bound forms of the dye after excitation at 380 nm. Basal cytosolic $[\text{Ca}^{2+}]$ values calculated as described above, for NTC and *STIM1* knockdown cells, were quantified as box plots. Quantification was from a minimum of 50 cells for all genotypes/treatment (except the wild-type untreated cells, $n = 25$) from 3 plates of each type. Statistical significance was computed using Mann-Whitney *U* test.

Immunocytochemistry and Quantitative Image Analysis

hESC-derived NPCs or spontaneously differentiating progenitors were fixed with 4% paraformaldehyde, permeabilized in 0.1% Triton X-100 and blocked with 4% FBS. The cells were incubated with primary antibodies overnight at 4°C, following which they were washed and incubated with fluorescent-labeled secondary antibodies for 2 h at 37°C, washed again and finally covered with 60% glycerol (v/v) for imaging with an Olympus IX73 (Olympus Corporation, Shinjuku, Tokyo, Japan) inverted microscope using 10X and 20X objective lenses. Images were analyzed and quantified using the Q-Capture Pro (RRID: SCR_014432) and ImageJ (RRID: SCR_003070) software, respectively. For confocal microscopy, an inverted Olympus FV1000 confocal microscope was used with a 60X oil objective, the Fluoview 2.1 C software (Olympus Fluoview FV10-ASW, RRID: SCR_014215) and FV10-SPD detectors, under optimal settings. Cell nuclei were counterstained with 300nM DAPI (4, 6-diamidino-2-phenylindole, Sigma) and 10–15 random fields from 3 to 4 plates were acquired for each immunostained sample. Student's unpaired *t*-test, assuming unequal variance, was used for *p*-value calculation from three independent experiments. Details of the primary antibodies used are as follows:

STIM1, 1:500 (Cell Signaling Technology Cat# 5668S, RRID: AB_10828699); Sox2, 1:150 (Abcam Cat# ab97959, RRID: AB_2341193); Tuj1, 1:1000 (Promega Cat# G7121, RRID: AB_430874); Sox1, 1:500 (Abcam Cat# ab87775, RRID: AB_2616563); Nestin, 1:500 (Abcam Cat# ab92391, RRID: AB_10561437); MAP2, 1:500 (Abcam Cat# ab32454, RRID: AB_776174); Doublecortin, 1:500 (Abcam Cat# ab18723, RRID: AB_732011); VIMENTIN, 1:500 (BD Biosciences Cat# 550513, RRID: AB_393716); TH, 1:2000 (Millipore Cat# AB152, RRID: AB_390204); Ki-67, 1:400 (Millipore Cat# AB9260, RRID: AB_2142366).

Library Preparation, Sequencing and RNA-Seq Data Analysis

Total RNA was isolated from hNPCs using TRIzol as per manufacturer's instructions. The RNA was run on a Bio-analyzer chip (Agilent) to ensure integrity. Approximately 500 ng of total RNA was used per sample to prepare libraries (RIN values > 9) using a TruSeq RNA Library Prep Kit v2 (Illumina) following manufacturer's instructions. The prepared libraries were run on a DNA1000 chip of a Bio-analyzer to check their size. Libraries were then quantified by qPCR and run on an Illumina HiSeq2500 platform, for a single end and 75 bp read protocol (SciGenom, India). Nine samples were run in a single lane. Biological triplicates were performed for each sample consisting of RNA isolated from wild-type NPCs, shRNA control NPCs (referred to as the Non-Targeting Control or NTC) and *STIM1* knockdown NPCs.

More than 100 million reads were obtained per sample with a uniform distribution of reads across samples (**Figure 3B**). FASTQ sequencing reads obtained were aligned to the annotated UCSC human genome (GRCh37/hg19) using HISAT2, RRID: SCR_015530 (Version-2.0.5) (Kim et al., 2015). These aligned SAM files were converted to BAM files using SAMtools (Version- 1.3) (Li et al., 2009). The resulting alignment data were then fed to CuffDiff2, RRID: SCR_001647, a software package that takes the reads aligned in BAM format as input, and uses geometric normalization on gene-length normalized read counts (FPKM, fragments per kilo base of exon per million reads), a beta negative binomial model for distribution of reads and *t*-test, for calling differentially expressed genes (Trapnell et al., 2012; Seyednasrollah et al., 2015). We set a corrected *p*-value, referred to as the *q*-value cut-off of 0.05 and Fold change > 1 = 1.5(+/-) to identify differentially expressed genes (DEGs) by this method. Read counts for each transcript or exon were also calculated independently using the Python based package HTSeq (Version 0.9.1) (Anders et al., 2015). These read counts were used as inputs for differential analysis with DESeq, RRID: SCR_000154 (Anders et al., 2015) and EdgeR (Empirical analysis of digital gene expression in R), RRID: SCR_012802 (Anders and Huber, 2010; Robinson et al., 2010), two R based Bioconductor software packages that analyze the read counts per transcript per sample and normalize them using the method of Trimmed Mean of *M*-values (TMM) for removing genes with very low read counts. DEGs were identified by fitting the values obtained in a negative binomial model, with variance and mean linked by local regression (Anders and Huber, 2010; Robinson et al., 2010; Lin et al., 2016). A fold change of 1.5 (+/-) and a *p*-value of 0.05 in DESeq and an FDR *p*-value of 0.05 were set as the cut-off in EdgeR. Genes found to be significantly altered by all the three differential gene expression analysis methods were considered further. Significantly up and downregulated genes were separately subjected to a gene ontology based gene enrichment analysis tool, DAVID (Version 6.8) (Database for Annotation, Visualization and Integrated Discovery) (Dennis et al., 2003) and FunRich (Functional enrichment analysis tool) (Pathan et al., 2015),

using the human genome as the background gene set. After converting the input gene IDs to corresponding DAVID gene IDs, the Functional Annotation Tool was used for gene enrichment analysis, based on the DAVID knowledge base. Fisher's exact *p*-value method was employed to measure gene-enrichment in DAVID, with a *P*-value cut-off of 0.1 and the count threshold kept at 2 to speculate maximum information. Most significant biological pathways (GO level 5) enriched in DAVID have been reported as bar graphs. Gene enrichment analysis was also performed using the human Gene Ontology database, HPRD2 and FunRich (Pathan et al., 2015). Here, selected biological processes were identified based on the presence of a higher percentage of genes (>6%). Genes enriched in each identified pathway have been represented as heat maps based on their FPKM values. The density box plot and dendrogram were generated using CummeRbund, RRID: SCR_014568 (Goff et al., 2012). Heat maps were generated using Matrix2png, RRID: SCR_011614 (Pavlidis and Noble, 2003) and HemI (Heatmap Illustrator, Version 1.0.3.7) (Deng et al., 2014). Comparison of significantly altered gene lists from CuffDiff, DESeq and EdgeR, and the generation of Venn Diagrams were performed using FunRich. The data discussed in this publication have been deposited in NCBI's Gene Expression Omnibus (Edgar et al., 2002) and are accessible through GEO Series accession number GSE109111.

Quantitative Real-Time PCR

RNA was isolated from cells using TRIzol as per manufacturer's instructions. Quantity of the isolated RNA was estimated by a NanoDrop spectrophotometer (Thermo Scientific). Approximately 1 µg of total RNA was used per sample for cDNA synthesis. Three or more independently isolated RNA samples were tested for validation of gene expression by quantitative PCR. Total RNA was treated with 0.5U of DNase I (amplification grade) in a reaction mixture (22.1 µl) containing 1 mM DTT and 20U of RNase inhibitor. The reaction mixture was kept at 37°C for 30 min followed by heat inactivation at 70°C for 10 min. To this, 200U of MMLV reverse transcriptase, 50 µM random hexamers, and 1 mM dNTPs were added in a final volume of 25 µl for cDNA synthesis. The reaction mixture was kept at 25°C for 10 min, then 42°C for 60 min, and finally heat inactivated at 70°C for 10 min. Quantitative real-time PCRs (qPCRs) were performed in a total volume of 10 µl with Kapa SYBR Fast qPCR kit (KAPA Biosystems) on an ABI 7500 fast machine operated with ABI 7500 software (Applied Biosystems). Duplicates were performed for each qPCR reaction. GAPDH was used as the internal control. The fold change of gene expression in any experimental condition relative to wild-type was calculated as $2^{-\Delta\Delta Ct}$, where $\Delta\Delta Ct = (Ct_{(target\ gene)} - Ct_{(GAPDH)})_{from\ STIM1\ knockdown\ cDNA} - (Ct_{(target\ gene)} - Ct_{(GAPDH)})_{from\ NTC\ cDNA}$. Four independent samples in addition to the samples used for the RNA-Seq were quantified for each gene. Statistical significance was determined by the unequal variance *t*-test. Primer sequences (F, forward primer and R, reverse primer) for each gene tested by qPCR are given below:

GAPDH F-TCACCAGGGCTGCTTTTAACTC
 R-ATGACAAGCTTCCCGTTCTCAG
STIM1 F-CACACTCTTTGGCACCTTCC
 R-TGACAATCTGGAAGCCACAG
UNC5C F-ACGATGAGGAAAGGTCTGCG
 R-AAGTCATCATCTTGGGCGGC
ELAVL3 F-CAAGATCACAGGGCAGAGC
 R-ACGTACAGGTTAGCATCCCC
DLG4 F-ACCAAGATGAAGACACGCC
 R-CCTGCAACTCATATCCTGGGG
NFAT4 F-CCGTAGTCAAGCTCCTAGGC
 R-TCTTGCCTGTGATACGGTGC
LIN28A F-AAGAAGTCAGCCAAGGGTCTG
 R-CACAGTTGTAGCACCTGTCTC
BAX F-CGGGGTTTCATCCAGGATCG
 R-CGGCAATCATCCTCTGCAGC

Western Blots

For total protein quantification, cells were lysed using a 1X cell lysis buffer (Cell Signaling Technologies) with protease inhibitors and phosphatase inhibitors as per manufacturer's protocol. Protein quantity was estimated by the Bradford assay and an equal amount of protein was loaded for immunoblotting. Proteins were transferred onto nitrocellulose membranes. The blots were blocked with 5% skimmed milk or bovine serum albumin for an hour at 37°C. After blocking, the blot was incubated with a primary antibody overnight at 4°C and probed with the respective secondary antibody conjugated to horseradish peroxidase (HRP), by incubation for an hour at 37°C. Antibodies for STIM1 and DCX were used at 1:1000 dilutions, Tuj1 at 1:2000, Sox2 at 1:300 (RRIDs provided in the section on immunocytochemistry above), and Actin (Loading control) at 1:3000 (BD Biosciences Cat# 612656, RRID: AB_2289199). Secondary antibodies used were anti-mouse HRP (1:3000; Cell Signaling Technology Cat# 7076, RRID: AB_330924) and anti-rabbit HRP (1:3000; Thermo Fisher Scientific Cat# 32260, RRID: AB_1965959). Bands were visualized with a chemiluminescence kit (GE Healthcare, Little Chalfont, United Kingdom) and captured using a chemiluminescent detection system (ECL, Thermo Scientific) with ImageQuant software (RRID: SCR_014246). Blots have been cropped for presentation in the main figures. Original images of the blots used are shown in **Supplementary Figure S3**. Unequal variance *t*-test was performed on band densities, obtained after background-subtraction, from at least three independent experimental blots.

Neurosphere Formation Assay

H9-derived NPCs, both control (NTC) and *STIM1* knockdown cells, were seeded into 96-well plates at a density of 50 cells/ μ l per well. Fresh medium was added every other day, and spheres were counted after 1 week. The total numbers and the average size of neurospheres were counted from bright-field images of each independent condition performed as replicates.

Statistical Analyses

For comparison between two samples, a two-tailed unpaired Student's *t*-test was used and the *p*-value is stated in the respective figures and figure legends. All statistical tests were performed using Origin 8.0 software (RRID: SCR_014212). Mann-Whitney *U* test after applying the Bonferroni correction was used for the Ca²⁺ Imaging data. The Fischer exact *P*-value was used for RNA-Seq data analysis, after Benjamini-Hochberg procedure and Bonferroni correction. Statistical tests are also explained in the respective method sections. All data are pooled from three or more independent experiments and are presented as mean \pm SEM. Asterisks indicate (*) *p* \leq 0.05, (**) *p* \leq 0.01 and (***) *p* \leq 0.001. Final figures were made in Adobe Photoshop (RRID: SCR_014199) or Inkscape (RRID: SCR_014479).

RESULTS

Derivation of Expandable Neural Precursor Cells (NPC) From Human Embryonic Stem Cells (hESC)

Neural differentiation of human Embryonic Stem Cells (hESCs) relies on an enhanced understanding of developmental signaling mechanisms that drive neurogenesis in a physiological context (Yap et al., 2015). The use of small molecules to successfully induce neural differentiation and to generate neural precursors *in vitro* has been established reproducibly in multiple cases (Efe and Ding, 2011; Li et al., 2011; Chambers et al., 2012; Neely et al., 2012). We derived neural precursors from hESCs (**Figure 1A**) by a dual SMAD inhibition protocol where rapid neuroectoderm differentiation was induced by inhibition of BMP and TGF β signaling (Reinhardt et al., 2013). To maintain the developmental potential for both neural crest and neural plate, Shh signaling was inhibited in the differentiating embryoid bodies (EBs) and a GSK3 β inhibitor was included to stimulate canonical Wnt signaling (Reinhardt et al., 2013). EBs in suspension exhibited epithelial outgrowths (**Figure 1B**) and formed homogeneous colonies when plated on Matrigel after disaggregation. Neuro-epithelial cells (**Figure 1C**) thus derived could be passaged and maintained for more than 25 passages without any changes in cell kinetics. The cells expressed biomarkers of neural precursors such as Nestin, Sox1, and Sox2 (**Figures 1D–F**). Robust expression of the STIM1 (**Figure 1G**) protein (but not STIM2, data not shown) was also observed along with the proliferation antigen Ki-67 (**Figure 1H**). Because the NPCs were not derived by rosette-based manual selection (Zhang et al., 2001; Elkabetz et al., 2008), chromosome stability of P10 metaphasic NPCs was analyzed. The karyotype appeared normal (**Figure 1I**) indicating that small molecule and enzymatic treatment used for deriving the NPCs did not incur chromosomal aberrations. The cells exhibited good post-thaw recovery rates after cryopreservation. Their cell-growth kinetics and marker expression profiles were reproducible after several freeze-thaw cycles and from different passages (data not shown). Upon withdrawal of the small molecules from the media, rapid neural differentiation was seen as evident from

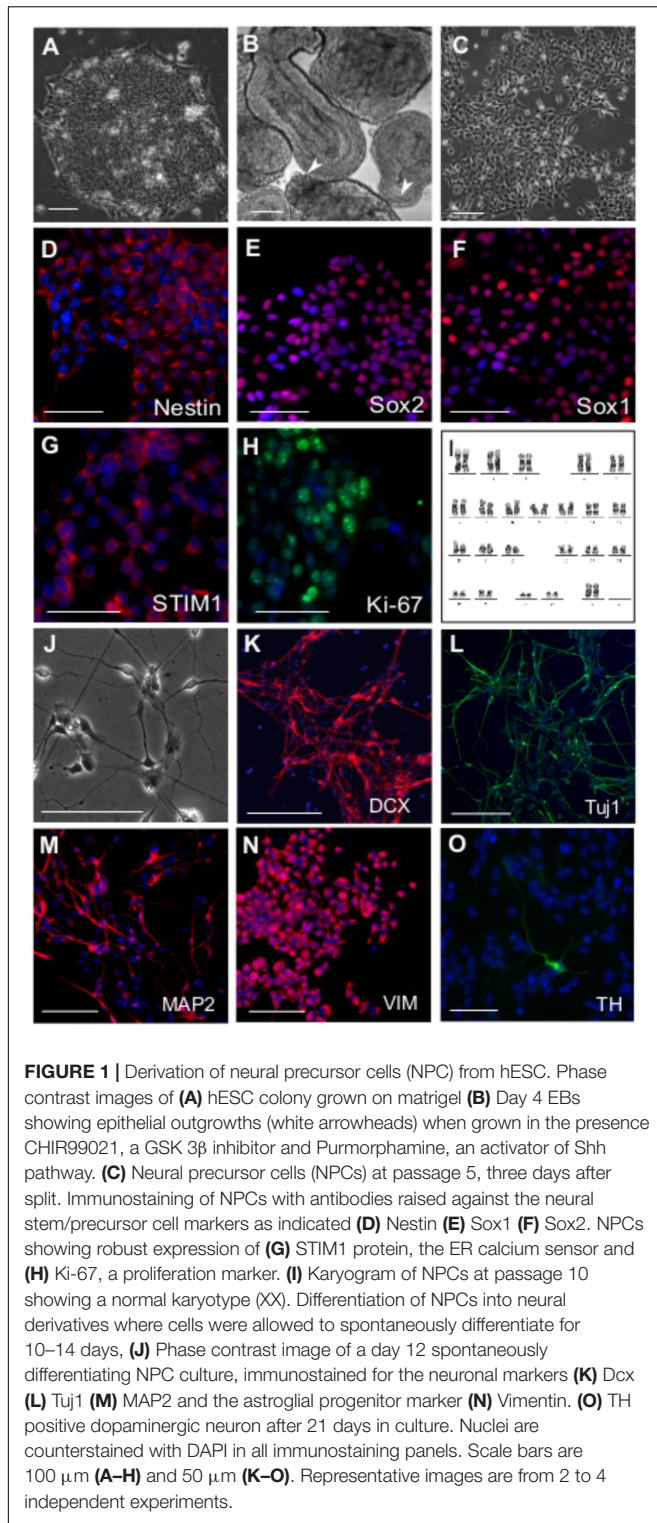


FIGURE 1 | Derivation of neural precursor cells (NPC) from hESC. Phase contrast images of (A) hESC colony grown on matrigel (B) Day 4 EBs showing epithelial outgrowths (white arrowheads) when grown in the presence CHIR99021, a GSK 3 β inhibitor and Purmorphamine, an activator of Shh pathway. (C) Neural precursor cells (NPCs) at passage 5, three days after split. Immunostaining of NPCs with antibodies raised against the neural stem/precursor cell markers as indicated (D) Nestin (E) Sox1 (F) Sox2. NPCs showing robust expression of (G) STIM1 protein, the ER calcium sensor and (H) Ki-67, a proliferation marker. (I) Karyogram of NPCs at passage 10 showing a normal karyotype (XX). Differentiation of NPCs into neural derivatives where cells were allowed to spontaneously differentiate for 10–14 days, (J) Phase contrast image of a day 12 spontaneously differentiating NPC culture, immunostained for the neuronal markers (K) Dcx (L) Tuj1 (M) MAP2 and the astroglial progenitor marker (N) Vimentin. (O) TH positive dopaminergic neuron after 21 days in culture. Nuclei are counterstained with DAPI in all immunostaining panels. Scale bars are 100 μ m (A–H) and 50 μ m (K–O). Representative images are from 2 to 4 independent experiments.

expression of neuroblast and post-mitotic neuronal markers DCX (Doublecortin), Tuj1 (Neuron-specific Class III β -tubulin) and MAP2 (Microtubule Associated Protein-2) in neuronal progenitors (Figures 1J–M), along with astroglial progenitors marked by Vimentin (Figure 1N). However, in agreement with

previous findings astroglia-like cells appeared much later (at least after 7 days of differentiation) than their neuronal counterparts and were restricted to smaller areas in the culture dish (Qian et al., 2000). Interestingly, such spontaneous differentiation also yielded a few dopaminergic neurons as indicated by immunostaining with an antibody to Tyrosine Hydroxylase (TH) (Figure 1O).

SOCE in hNPCs and Its Attenuation With *STIM1* shRNA-miR

To determine whether small molecule-derived NPCs exhibit SOCE, we depleted ER stores using 10 μ M thapsigargin (TG), an inhibitor of the sarcoendoplasmic reticulum Ca^{2+} ATPase pump (Lytton et al., 1991) in a Ca^{2+} -free solution and studied Ca^{2+} influx after re-addition of extracellular 2 mM Ca^{2+} . ER-store Ca^{2+} release, followed by SOCE after re-addition of external Ca^{2+} was observed consistently across several passages in human NPCs (Figure 2A). CRAC (calcium release-activated calcium) channels, identified as Orai1, and distinguished by high Ca^{2+} selectivity and a unique pharmacological profile (Feske et al., 2006; Lewis, 2011; McNally and Prakriya, 2012; Jairaman and Prakriya, 2013; Prakriya and Lewis, 2015) function in mouse NPCs as Store-Operated Calcium entry channels (Somasundaram et al., 2014). Therefore, we tested if potent CRAC channel inhibitors like BTP-2 (Ohga et al., 2008) and 2-aminoethoxy-diphenyl borate (2-APB, Prakriya and Lewis, 2001) affect SOCE in human NPCs. Both BTP-2 (Bootman et al., 2002) and 2-APB significantly inhibited SOCE in human NPCs (Figures 2B,C). Thus, the pharmacological profile of SOCE in human NPCs is consistent with that of CRAC channels and resembles SOCE in primary mouse NPCs (Somasundaram et al., 2014; Prakriya and Lewis, 2015).

In order to knockdown *STIM1* expression, NPCs (P10–P12) were transduced with *STIM1* shRNA lentiviral particles (Auyeung et al., 2013; Knott et al., 2014). Direct visual confirmation of induced shRNA expression through ZsGreen and rapid selection of transduced NPCs with Puro^R enabled efficient propagation of the transduced cells. Human NPCs transduced with a non-targeting vector control (NTC) were used as controls for all subsequent experiments. Western blot analyses confirmed maximal *STIM1* knockdown (>90%, $p = 0.00067$) in NPCs transduced with a pool of three *STIM1* targeting shRNAs (Figure 2D and Supplementary Figure S3A). Subsequent experiments were performed with NPCs at P18–P22. NPCs with *STIM1* knockdown (henceforth referred to as *STIM1* knockdown) exhibited a significant reduction in SOCE as compared to the corresponding control, whereas release of store Ca^{2+} , after inhibition of the sarcoplasmic ER Ca^{2+} -ATPase by thapsigargin treatment, appeared similar to control cells (Figures 2E,F). The mean basal cytosolic calcium levels in control and *STIM1* knockdown cells were 38 and 32 nM respectively (Figure 2G). Thus, *STIM1* knockdown causes a small but statistically significant reduction in basal [Ca^{2+}]. Reduced basal cytosolic Ca^{2+} was earlier reported after *STIM1* knockdown in HeLa cells (Brandman et al., 2007) and in HUVEC cells (Tsai et al., 2014).

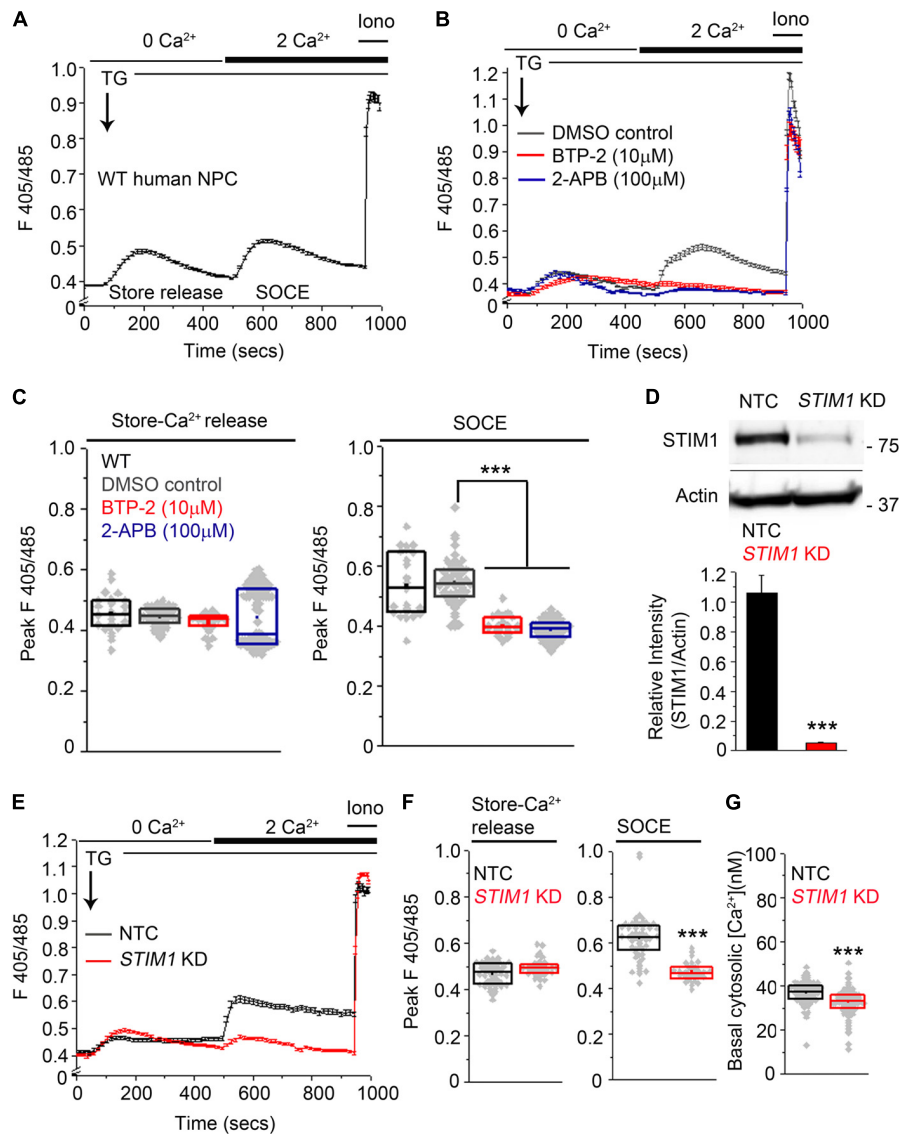
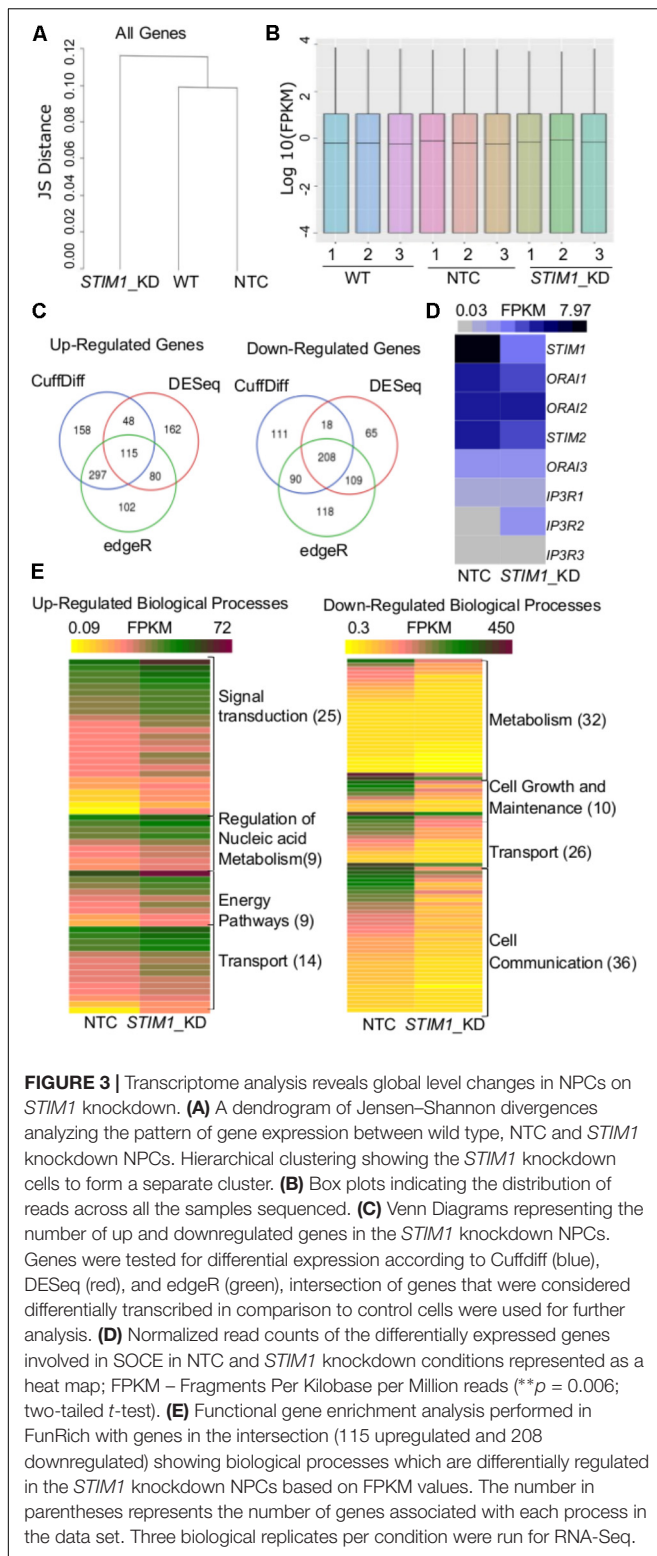


FIGURE 2 | Knockdown of *STIM1* attenuates SOCE in human NPCs. **(A,B)** Ca^{2+} -responses during ER-store release and SOCE induced by Thapsigargin (TG, 10 μM) measured using the ratiometric Ca^{2+} -indicator indo-1-AM in wild-type (WT) hNPCs **(A)** or hNPCs treated with pharmacological inhibitors of SOCE, BTP-2 and 2-APB at the indicated concentrations or DMSO as a solvent control **(B)**. Each trace represents the mean \pm SEM for 25–100 cells. Ionomycin (Iono, 10 μM) was added at the end of each imaging to determine the peak F405/485 ratio obtained after saturation of the Ca^{2+} -indicator with Ca^{2+} . **(C)** Box plots quantifying the peak F405/485 values for store-release and SOCE in the indicated treatment conditions. Mann–Whitney *U* test with Bonferroni correction. $p = 1.819 \times 10^{-23}$ for DMSO control compared to BTP-2 treatment and $p = 1.442 \times 10^{-45}$ for DMSO control compared to 2-APB treatment. **(D)** (Top) A representative Western blot showing levels of *STIM1* protein in hNPCs transduced with an NTC (non-targeting control) or an sh-RNA targeting *STIM1* (*STIM1* KD). Actin serves as the loading control. (Bottom) Quantification of *STIM1* band intensities normalized to the loading control Actin from three independent biological replicates ($p = 0.00069$, Student's *t*-test). **(E)** Ca^{2+} -responses during store-release and SOCE in hNPCs transduced with NTC and *STIM1* KD. **(F)** Box plots quantifying the peak F405/485 values for store-release and SOCE in the indicated genotypes. Peak F405/485 for store-release were not significantly different between NTC and *STIM1* KD NPCs. $p = 0.0001$ for peak F405/485 during SOCE compared between NTC- and *STIM1* KD NPCs. **(G)** Quantification of basal cytosolic $[\text{Ca}^{2+}]$ values using Fura-2-AM in NTC- and *STIM1* KD NPCs ($p = 1.115 \times 10^{-8}$, Mann–Whitney *U* test. (***)Indicates $p < 0.001$).

Transcriptional Profiling of *STIM1* Knockdown NPCs

The regulation of cell-specific gene expression by SOCE has been described in both non-excitable (Feske et al., 2001, 2005; Gwack et al., 2007) and neuronal cells (Mao et al., 2007; Lalonde et al., 2014; Somasundaram et al., 2014;

Pathak et al., 2015; Richhariya et al., 2017). To identify potential novel gene expression changes by *STIM1* knockdown in human NPCs, we performed parallel genome-wide analysis of mRNA expression profiles in non-transduced NPCs, NTC and the *STIM1* knockdown NPCs. Stable knockdown of *STIM1* leads to global transcriptional changes as evident by the clustering

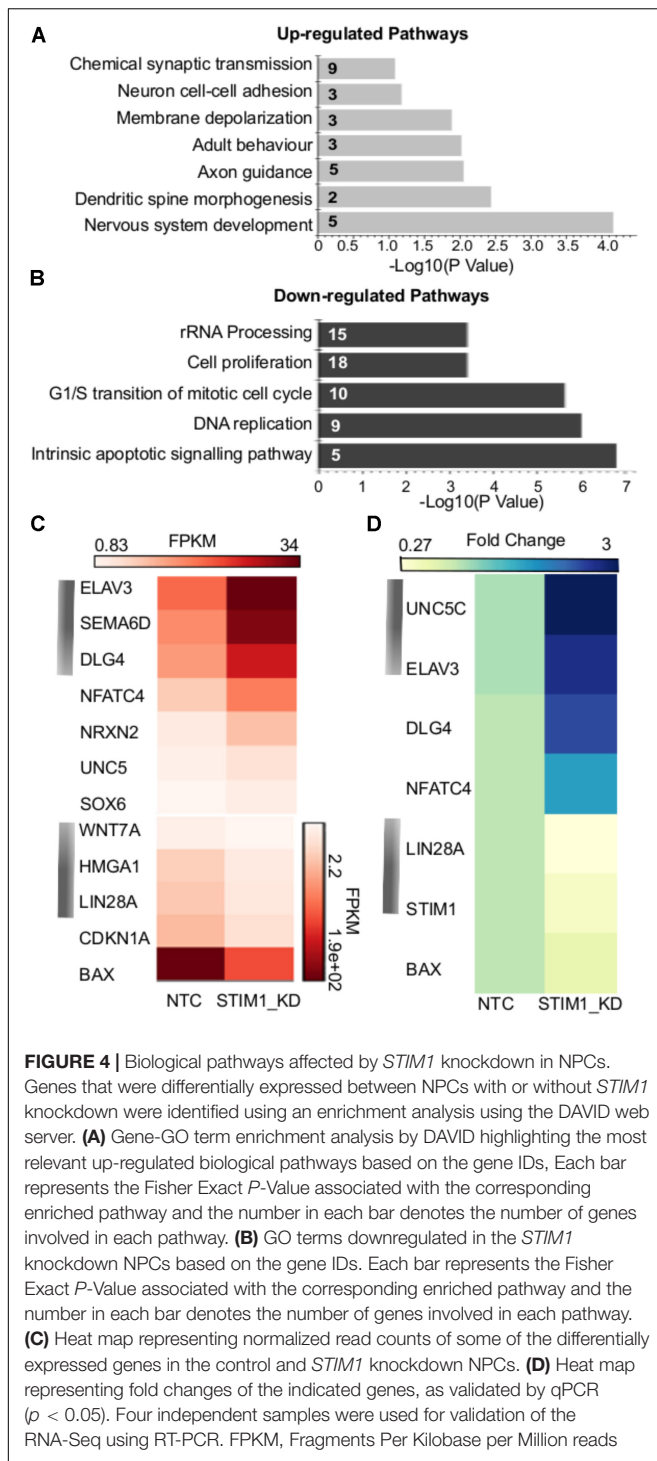


together of non-transduced NPCs with the NTC, whereas the *STIM1* knockdown formed a separate cluster with the Jensen-Shannon divergence as a metric (Figure 3A). The distribution of reads was uniform in all samples (Figure 3B). Three independent

methods, CuffDiff (Trapnell et al., 2012), EdgeR (Robinson et al., 2010), and DESeq (Anders and Huber, 2010) were used for differential expression analysis. Amongst the differentially expressed genes (DEGs) in *STIM1* knockdown NPCs, we further analyzed 115 up-regulated and 208 down-regulated genes, identified by their overlap from all three methods (Figure 3C). To understand if *STIM1* knockdown modulates expression of *STIM2* and the SOCE channel *Orai*, we looked at the FPKM values of these genes and confirmed that *STIM1* was the only gene that was significantly down-regulated (Figure 3D). Furthermore, we evaluated expression levels of the IP₃R sub-types because STIMs and the IP₃Rs are both located on the ER (Béliveau et al., 2014; Thillaiappan et al., 2017), where IP₃R-mediated Ca²⁺-release leads to STIM activation. Transcript levels of three IP₃R isoforms too did not change significantly in *STIM1* knockdown NPCs (Figure 3D). Hence the altered gene profiles of the *STIM1* knockdown hNPCs were not associated with two other classes of SOCE-related genes.

The nature of biological processes that might be affected by *STIM1* knockdown was predicted next by analysis of the DEGs. Up-regulated genes associated with biological processes such as signal transduction, regulation of nucleic acid metabolism and energy pathways, whereas down-regulated genes clustered with metabolism, cell growth and maintenance, and cell communication (Figure 3E). Genes regulating cellular transport were both up- and down-regulated (Figure 3E). The down-regulated processes appeared consistent with a less proliferative state, whereas the up-regulated processes suggested increased cellular specialization and differentiation (Karsten et al., 2003). To understand the nature of signaling mechanisms regulated by *STIM1* in hNPCs, we used DAVID to assess the Gene Ontology (GO) of DEGs. Biological pathways that were significantly up-regulated in *STIM1* knockdown NPCs relative to control NTCs appeared consistent with neuronal differentiation and included nervous system development (GO:0007399), membrane depolarization (GO:0051899), neuron cell-cell adhesion (GO:0007158) and chemical synaptic transmission (GO:0007268) (Figure 4A). Conversely, significantly down-regulated pathways in *STIM1* knockdown NPCs suggested reduced cell proliferation and included rRNA processing (GO:0006364), cell proliferation (GO:0008283), G1/S transition of mitotic cell cycle (GO:0000082) and DNA replication (GO:0006260) (Figure 4B) (Table 1). Intrinsic apoptotic signaling pathway in response to DNA damage by p53 class mediator (GO: 0042771) (Figure 4B) was also found to be significantly down-regulated suggesting that *STIM1* knockdown NPCs do not undergo apoptosis.

Gene expression changes of a few candidate genes are depicted in Figure 4C and some of these were chosen for further validation by quantitative PCR (Figure 4D). Markers of neuronal specification such as *Unc5c* (Kennedy et al., 1994), *Elavl3* (Ince-Dunn et al., 2012) and *Dlg4* (also known as the post-synaptic density protein 95, Feng and Zhang, 2009) were up-regulated more than 2.5 fold in *STIM1* knockdown NPCs (Figure 4D and data not shown). *Lin28a* and *Bax* were downregulated significantly with a fold change of 5.0 and 1.6 in the *STIM1* knockdown samples (Figure 4D, data not shown).



Lin28 is an RNA-binding protein enriched in early NPCs and its expression declines during neural differentiation (Yang et al., 2015). Interestingly, Bax initially identified as a pro-apoptotic member of the Bcl-2 family is also shown to regulate Ca^{2+} efflux from the ER, thus influencing Ca^{2+} -mediated apoptosis (Scorrano et al., 2003). These data support the hypothesis that *STIM1* knockdown in the NPCs reduces their proliferative and

self-renewal capacities and concomitantly induces premature neural differentiation.

***STIM1* Knockdown Leads to Decreased Proliferation and Early Differentiation of NPCs**

Based on analysis of the RNA-Seq data, we examined the morphology and proliferative potential of *STIM1* knockdown NPCs. *STIM1* knockdown cells exhibited rapid spontaneous differentiation evident as branched neurites and sparse cell clustering. The control NTC cells, however, resembled wild-type NPCs (compare **Figures 5A,B**). Their growth rates were similar to that of wild type cells (~24 h population doubling time, passaged every 3–4 days). In contrast, *STIM1* knockdown NPCs cultures took much longer (>7 days) to become confluent and exhibited slower growth as compared with NTCs (**Supplementary Figures S2A,B**). Reduced confluence of *STIM1* knockdown cells might arise from their premature commitment to a more differentiated phenotype and consequently a reduction in the number of undifferentiated NPCs, that are required for repopulating the culture. To obtain a measure of the self-renewal capacity of *STIM1* knockdown cells as compared to NTCs, both were tested by a neurosphere formation assay (Reynolds and Weiss, 1992; Pacey et al., 2006). Neural stem cells are known to continuously divide in culture to generate non-adherent spherical clusters of cells, commonly referred to as neurospheres when appropriate plating densities are established (Bez et al., 2003). Differences in the clonal-proliferation ability of *STIM1* knockdown cells were seen as early as 24 h, when very few cell-clusters were visible as compared to the NTCs (data not shown). At 48 h neurospheres were visible in both NTCs and *STIM1* knockdown cultures; however, neurosphere size was greatly reduced in the *STIM1* knockdown condition (compare **Figure 5D** with **Figure 5C**). This impaired proliferation was quantified by counting neurospheres generated after a week in culture. Neurosphere numbers were reduced to less than half of the NTC number in the *STIM1* knockdown cells (**Figure 5E**). Moreover, neurospheres that formed in the NTC cultures were larger in size ($180.0 \pm 8.3 \mu\text{m}$), irrespective of the general heterogeneity in sphere sizes across cultures, as compared with neurospheres in *STIM1* knockdown cultures ($76.0 \pm 4.32 \mu\text{m}$) (**Figures 5F,G**). The percentage of bigger spheres also appeared reduced in *STIM1* knockdown cells. Very small spheres (<50 μm) in both conditions were not scored. It is evident from these experiments that similar to mouse embryonic and adult NPCs (Somasundaram et al., 2014) the clonogenic and proliferative capacities of human NPCs are impaired upon *STIM1* knockdown.

Premature differentiation and the reduced proliferative potential of *STIM1* knockdown NPCs were further assessed by immunostaining with appropriate markers. The nuclear Ki-67 protein (pKi-67) has been shown to express exclusively in proliferating cells (Scholzen and Gerdes, 2000). More than 80% of control cells (NTC) were positive for Ki67 suggesting that they are dividing actively, whereas in *STIM1* knockdown cells just 30% were positive for Ki67 (**Figures 6A–C**). PCNA (proliferating cell

TABLE 1 | Biological pathways enriched by DAVID in *STIM1* KD hNPCs.

Go term	Pathway	P-value	Fold enrichment	Bonferroni	Benjamini	FDR	Genes
Upregulated							
GO:0007268	Chemical synaptic transmission	6.96E-05	6.491	0.038	0.019	0.101	NRXN2, KIF5A, NPTX2, GRIK4, DLG4, CHRNA4, PRKCG, CACNB3, CACNA1B
GO:0007158	Neuron cell-cell adhesion	0.003	32.458	0.876	0.407	5.265	NRXN2, NLGN4X, ASTN1
GO:0051899	Membrane depolarization	0.008	20.773	0.993	0.637	12.289	CHRNA4, CACNB3, CACNA1B
GO:0030534	Adult behavior	0.009	19.974	0.995	0.598	13.201	NRXN2, NLGN4X, SHANK1
GO:0007411	Axon guidance	0.013	5.443	0.999	0.656	17.590	KIF5A, NGFR, UNC5C, CHL1, SLIT3
GO:0060997	Dendritic spine morphogenesis	#0.066	28.852	1.0	0.950	63.527	DLG4, SHANK1
GO:0007399	Nervous system development	#0.082	3.015	1.0	0.933	71.593	IGSF8, CPLX2, DLG4, SPOCK1, ELAVL3
Downregulated							
GO:0006364	rRNA processing	1.62E-07	6.130	2.21E-04	2.21E-04	2.66E-04	EMG1, PNO1, EXOSC5, RPS27L, DIEXF, MRT04, NOP14, EBNA1BP2, PA2G4, DKC1, DHX37, DDX21, PES1, LTV1, WDR43
GO:0008283	Cell proliferation	1.00E-06	4.301	0.001	6.82E-04	0.001	POLR3G, TP53, CD70, MCM10, PRDX1, CDC25A, PLCE1, PA2G4, DKC1, ASCC3, FRAT2, TXNRD1, NRG1, LRP2, PES1, MYC, EMP1, GNL3
GO:0000082	G1/S transition of mitotic cell cycle	2.43E-06	8.574	0.003	0.001	0.003	CCNE1, CDC6, CDC45, CDKN1A, RRM2, ID4, CDK6, RCC1, MCM10, CDC25A
GO:0006260	DNA replication	4.01E-04	5.078	0.420	0.127	0.655	EXO1, CDC6, CDC45, POLE3, RRM2, MCM10, C10ORF2, CDC25A, DSCC1
GO:0042771	Intrinsic apoptotic signaling pathway in response to DNA damage by p53 class mediator	4.01E-04	14.106	0.420	0.103	0.656	CDKN1A, AEN, TP53, RPS27L, PHLDA3

Top biological pathways up- and down-regulated in *STIM1* KD NPCs vs. control cells. Fisher Exact P-values are shown and GO terms are arranged according to their FDR value (False Discovery Rates). All over-represented pathways had a fold change > 2. Both Benjamini-Hochberg and Bonferroni multiple testing correction methods for the occurrence of false positive identifications by adjusting p-values are given. Shown are the gene lists identified in our data set and associated with each pathway. # Indicates p-value > 0.05.

nuclear antigen), another marker for proliferation in eukaryotic cells (Strzalka and Ziemienowicz, 2011) was also significantly down-regulated in the *STIM1* knockdown cells as evident from the RNA-Seq data (Fold change -1.4 , $p = 0.03$, GSE109111). In parallel with reduced expression of proliferation markers, several proteins related to neural differentiation were up-regulated in *STIM1* knockdown NPCs, where knockdown of *STIM1* protein was re-confirmed (Figure 6M and Supplementary Figure S3A). Expression of differentiation markers in the *STIM1* knockdown cells was analyzed within 7 days of culture. As in NTCs, we did not observe changes in the numbers of glial progeny. However, the ability of *STIM1* knockdown in NPCs, to alter glial fate and numbers could manifest at later stages of differentiation. This has not been tested.

Doublecortin (DCX) is a brain-specific microtubule-associated protein that regulates neuronal migration and is associated with neurogenesis (Francis et al., 1999). DCX levels were negligible in control cells whereas 35% of *STIM1*

knockdown cells expressed DCX (Figures 6D–F). Expression of DCX was further confirmed in *STIM1* knockdown cells by western blots (Figure 6O and Supplementary Figure S3C). Immunoreactivity of neuronal β III Tubulin, Tuj1 was also higher in *STIM1* knockdown cells ($85.0\% \pm 0.9$) as compared to NTCs ($\sim 35\%$). Moreover, *STIM1* knockdown NPCs expressing TUJ1 exhibit branched neurites, unlike the NTCs, where such neuronal morphology was not evident (Figures 6G–I, P and Supplementary Figure S3D). Expression of Sox2, a transcription factor required in part for the maintenance of NPC properties and functions, through the Shh and Notch pathways (Wegner, 2011) was tested next in *STIM1* knockdown NPCs. It is known that deletion of Sox2 in the mouse attenuates the self-renewal capacity of hippocampal NSCs (Favaro et al., 2009). Sox2-positive cells were somewhat lower in number in the *STIM1* knockdown cells (Figures 6J–L) and total Sox2 protein as measured by western blots was significantly reduced in *STIM1* knockdown NPCs (Figure 6N and Supplementary Figure S3B).

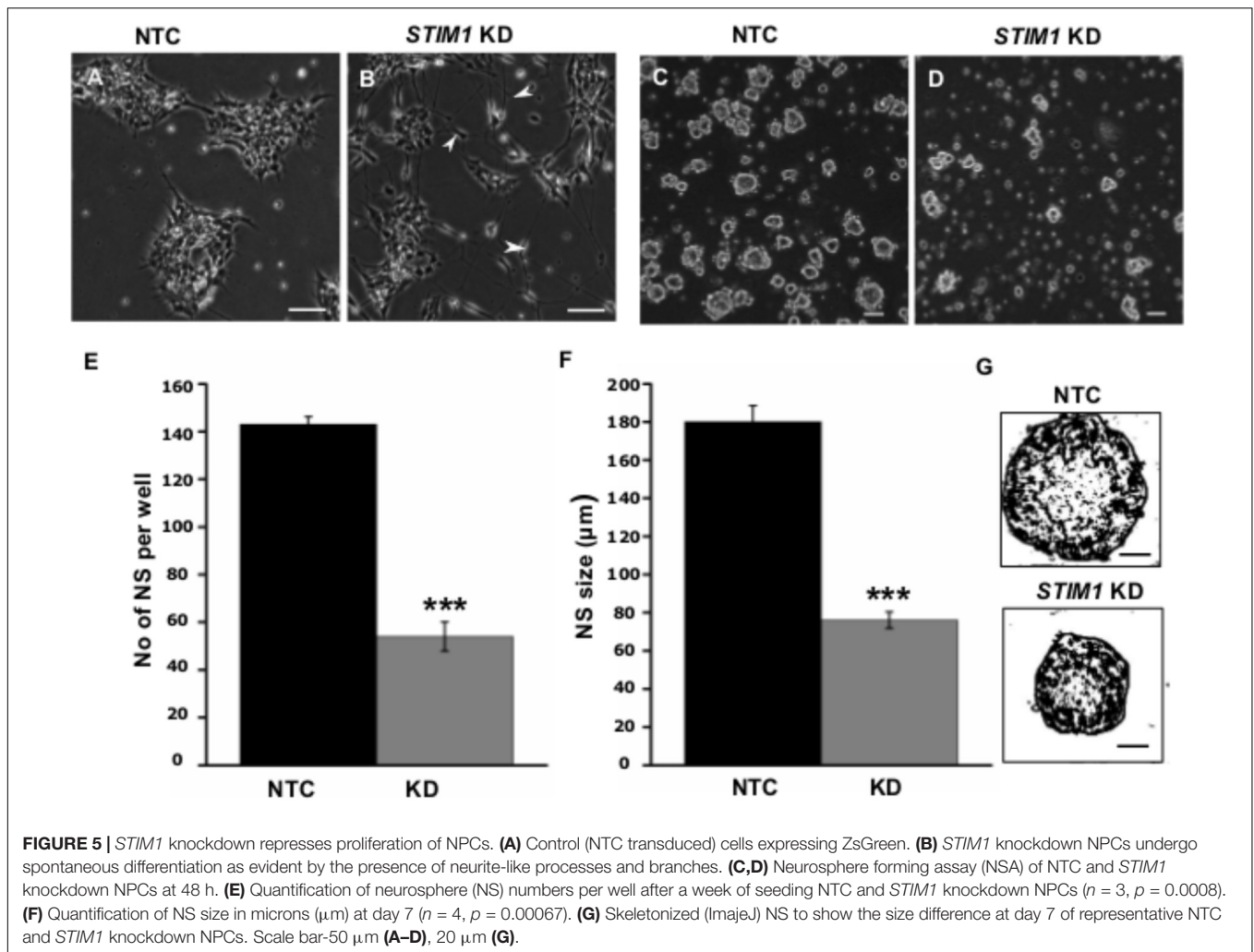


FIGURE 5 | *STIM1* knockdown represses proliferation of NPCs. **(A)** Control (NTC transduced) cells expressing ZsGreen. **(B)** *STIM1* knockdown NPCs undergo spontaneous differentiation as evident by the presence of neurite-like processes and branches. **(C,D)** Neurosphere forming assay (NSA) of NTC and *STIM1* knockdown NPCs at 48 h. **(E)** Quantification of neurosphere (NS) numbers per well after a week of seeding NTC and *STIM1* knockdown NPCs ($n = 3$, $p = 0.0008$). **(F)** Quantification of NS size in microns (μm) at day 7 ($n = 4$, $p = 0.00067$). **(G)** Skeletonized (ImajeJ) NS to show the size difference at day 7 of representative NTC and *STIM1* knockdown NPCs. Scale bar-50 μm **(A–D)**, 20 μm **(G)**.

Thus, *STIM1* knockdown in human NPCs induces early neural differentiation that would eventually deplete the NPC pool. Indeed, transcript levels of many neuronal (*NPY*, *NPTX2*, *DLG4*, *NLGN4X*, *NRXN2*, *CEND1*, *NEFH*, *NEUROG2*, *NEUROG1*) and some early glial markers (*HES5*, *SLC1A3*, *CD44*, *PDGFRA*) were also significantly up-regulated in the *STIM1* knockdown NPCs as evident from RNA-Seq data (**Figure 6Q**, GSE109111). Physiologically NPCs/NSCs need to fine-tune quiescence and proliferation/commitment to guarantee lifelong neurogenesis and avoid premature exhaustion (Cavallucci et al., 2016). Knockdown of *STIM1* appears to tip this balance and push the cells toward a differentiated phenotype.

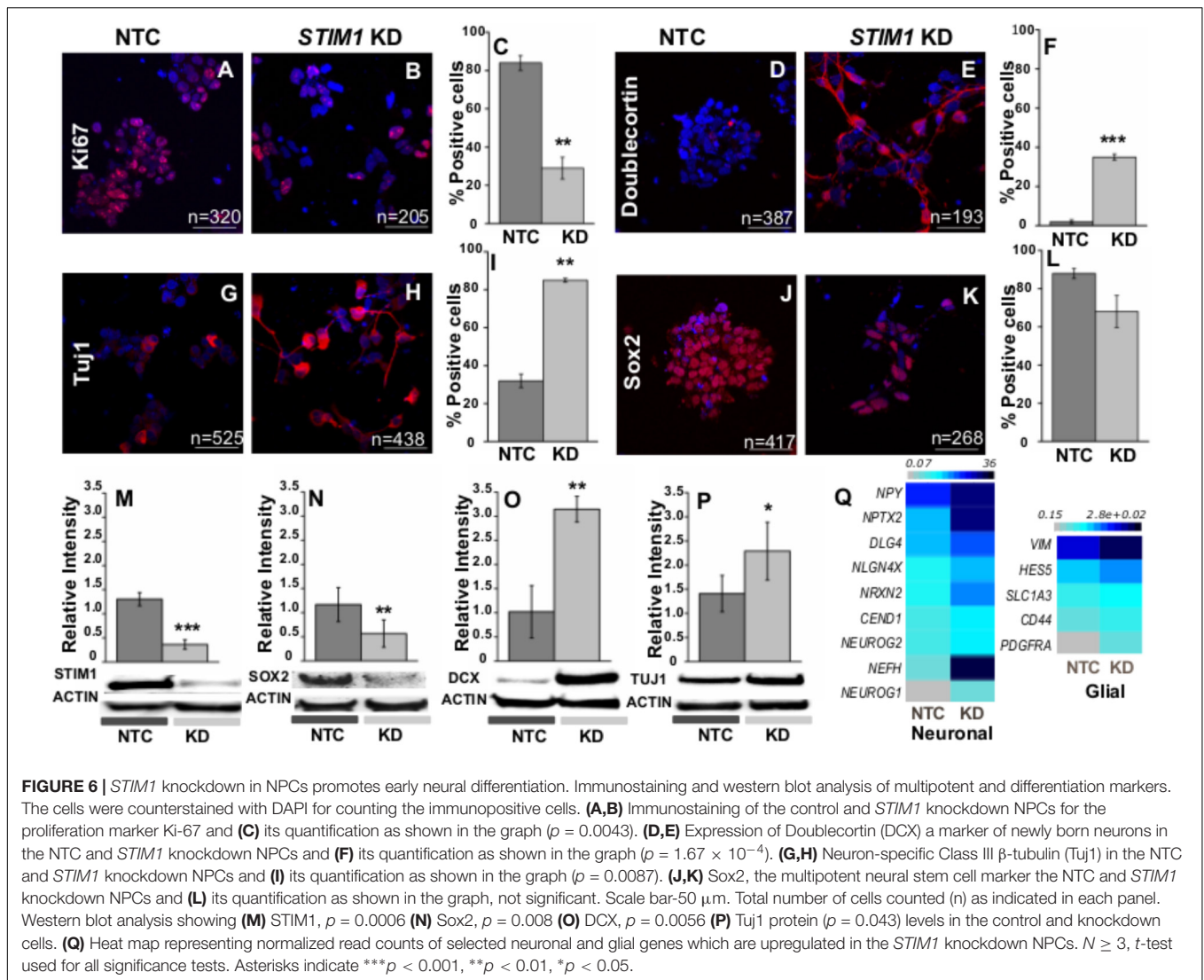
DISCUSSION

The ability of human neural precursor cells to maintain their proliferative potential and generate neurons or glia in a spatiotemporal manner is important in the context of multiple neurological and psychiatric disease conditions (Ishibashi et al., 1995; Elder et al., 2006; Shi et al., 2008; Cramer et al., 2011). In this study we have identified the ER Ca^{2+} sensor *STIM1*

as essential for Store Operated Calcium Entry (SOCE) in human NPCs. Global gene expression changes were observed in hNPCs after a stable knockdown of *STIM1* that is likely a consequence of reduced SOCE. *STIM1* knockdown in hNPCs reduced the expression of genes associated with cell proliferation and upregulated genes belonging to pathways for nervous system development and differentiation. Furthermore, morphological and immunohistochemical analyses identified a fate change in *STIM1* knockdown NPCs where the balance between self-renewal and differentiation was altered significantly toward the latter. Mouse neural precursors with loss of function of the SOCE channel Orai exhibit very similar fate changes (Prakriya et al., 2006; Lewis, 2007; Domenichini et al., 2018).

Role of ER Ca^{2+} and SOCE in Mammalian Neurogenesis

Ca^{2+} signals affect the earliest steps of neurogenesis including neural induction, differentiation of neural progenitors into neurons, and the neuro-glial switch (Leclerc et al., 1997, 2000, 2012). The endoplasmic reticulum (ER) is a major



Ca^{2+} storage organelle that contributes to multiple Ca^{2+} signaling pathways. In hESC-derived neural progenitors, Ca^{2+} mobilization from intra- and extracellular compartments occurs in response to depolarization and by activation of glutamatergic and dopaminergic receptors (Malmersjö et al., 2010). In agreement with published data demonstrating purinergic, ATP- and glutamate-induced $[\text{Ca}^{2+}]_i$ responses in hNPCs (Forostyak et al., 2013) RNA-Seq analysis of hNPCs derived in this work confirmed purinergic receptor expression (*P2RX3*, *P2RX4*, *P2RY1* and *P2RY11*) at FPKM > 3 and robust expression of an ionotropic glutamate receptor (*GRINA* or *NMDARA1*: FPKM > 90). Expression of several subclasses of TRP channels (*TRPC1*, *TRPC4*, *TRPM4*, *TRPM7*, *TRPV1*) (FPKM > 3) was also evident (GSE109111). Interestingly the neural 'N' type voltage-gated Ca^{2+} channel *CACNA1B* and the β subunit *CACNB3* present in hNPCs (FPKM > 2) showed significant upregulation in *STIM1* knockdown (GSE109111) possibly as a compensatory mechanism for maintaining cellular Ca^{2+} homeostasis. Upregulation of a TRP channel has been

observed in IP_3 receptor mutant neurons of *Drosophila* where it appears to compensate for changes in cellular calcium homeostasis (Chakraborty and Hasan, 2017). Moreover, Calreticulin, a luminal Ca^{2+} buffering protein in the ER is also regulated upon neural differentiation in mouse ESCs (Wang and Gao, 2005). Thus, stage-specific regulation of ER Ca^{2+} -release and SOCE impacts neuronal development across invertebrates and vertebrates and appears essential for neural differentiation of neural precursors in mammals including humans.

The physiological significance of neuronal SOCE in neural precursors requires further investigation particularly in the context of neurological disorders. The RNA-Seq data demonstrate that hNPCs also express several classes of receptor tyrosine kinases belonging primarily to the FGF and EGF receptors families that are known to activate Ca^{2+} signaling through Phospholipase $\text{C}\gamma$, some of which are differentially expressed in the *STIM1* knockdown NPCs. The reduced proliferative potential of *STIM1* knockdown NPCs might

derive from altered expression of receptor tyrosine kinases (GSE109111). Transcriptional profiling downstream of reduced SOCE, as reported here, is a first step in understanding the cellular and molecular mechanisms underlying SOCE-related human neurological disorders and the use of pluripotent cell-derived NPCs for disease modeling and cell-based therapies (Brafman, 2015).

STIM1 Affects Self-Renewal of Human NPCs

Neural stem cells (NSCs) or neural precursor cells (NPCs) (first reported by Altman and Das, 1965) *in vivo* are derived from the nervous system, can self-renew and can give rise to cells other than themselves through asymmetric cell division (Gage, 2000). NPCs require a specific metabolic state to maintain the balance between self-renewal and differentiation and decreased metabolic demand and impaired renewal is associated with various brain disorders (Knobloch et al., 2013; Kim et al., 2014). Proliferative stem cells in mammalian and *Drosophila* nervous systems are highly anabolic. Their high levels of lipogenesis and decreased amino acid and lipid oxidation regulate cell proliferation and determine cell fate (Knobloch et al., 2013; Homem et al., 2014, 2015). SOCE also contributes to metabolic reprogramming of naive T cells by regulating expression of components of the PI3K-AKT kinase-mTOR nutrient-sensing pathway (Vaeth et al., 2017). It is possible that reduced cell metabolism, one of the biological processes, enriched in our study (Figure 3E) leads to decreased cell proliferation of the *STIM1* knockdown cells. Knock-down of *STIM1* and *Orai1* also inhibit proliferation of vascular smooth muscle cells (Potier et al., 2009) and knockdown of either *STIM1*, *STIM2* or *Orai1* inhibit endothelial cell proliferation leading to cell cycle arrest at S and G2/M phase (Abdullaev et al., 2008). Several other studies suggest that SOCE and metabolism are interlinked. Astrocytic glycogenolysis in murine cerebellar and cortical cultures is stimulated by SOCE (Muller et al., 2014). In *Drosophila*, altered lipid metabolism has been described in mutants with attenuated Ca^{2+} -release through the IP₃R and reduced SOCE (Subramanian et al., 2013; Baumbach et al., 2014). A cell-intrinsic role of SOCE in regulating lipid metabolism in mice and cells from human patients defective in SOCE has also been shown (Arruda et al., 2017; Maus et al., 2017). Together these data suggest that *STIM1* and SOCE support a high-energy metabolic state in various cells including NPCs, which in turn facilitates cell proliferation.

Relevance to Neurodevelopmental and Neuropsychiatric Disorders

Mammalian neuroepithelial cells or NPCs *in vivo*, initially undergo symmetric proliferative divisions (Rakic, 1995) to expand their population and later switch to asymmetric divisions that produce more of themselves and a lineage specified downstream cell (Huttner and Kosodo, 2005; Florio and Huttner, 2014). The transition from symmetric to asymmetric division is tightly regulated, and precocious asymmetric divisions result

in premature differentiation and smaller brains (Cabernard and Doe, 2009; Gauthier-Fisher et al., 2009; Egger et al., 2010). Aberrant NPC regulation is now linked to many developmental and degenerative disorders of the brain (reviewed by Ladran et al., 2013). The stable knockdown of *STIM1* significantly reduced NPC proliferation concurrently inducing their spontaneous differentiation to neural progenitors. In a systemic context, this phenotype might lead to an early cessation of the stem cell pool in the brain and differentiated neural cell types that are likely to be dysfunctional or exhibit sub-optimal functions. Interestingly patients with *STIM1* mutations in the EF hand or CC domains have been reported recently with psychiatric disturbances (Harris et al., 2017). Moreover, in a large genome-wide analysis of psychiatric patients by Cross-Disorder Group of the Psychiatric Genomics Consortium (2013), dysregulated Ca^{2+} homeostasis was identified in several disorders. In this context, neurodevelopmental aberrations arising from abnormal specification, growth, expansion and differentiation of embryonic NPCs are thought to contribute to neurological disorders that initiate in childhood as well as toward certain adult-onset mental disorders, including autism, language disorders and mental retardation (Stevens et al., 2010). In differentiated neurons, SOCE is thought to regulate neuronal gene expression (Lalonde et al., 2014), and the maturation and maintenance of dendritic spines (Sun et al., 2014; Korkotian et al., 2017). Defective SOCE has been associated with several neurodegenerative disorders, such as Huntington's disease (Nekrasov et al., 2016; Wu et al., 2011, 2016), Alzheimer's disease (Leissring et al., 2000; Yoo et al., 2000; Zhang et al., 2015), Parkinson's disease (Zhou et al., 2016), spongiform encephalopathies (Lazzari et al., 2011) and chorea-acanthocytosis (Pelzl et al., 2017). In the light of our findings in NPCs, it is tempting to speculate that deficient SOCE alters neuronal gene expression patterns in a temporal manner resulting in disease pathologies that manifest over several years. Further investigation of *STIM1* function and SOCE in neurodevelopmental, neurodegenerative and psychiatric disorders could thus generate novel therapeutic insights.

AUTHOR CONTRIBUTIONS

RG designed and performed the experiments and wrote the manuscript. BD performed the experiments and edited the manuscript. PC performed the experiments, analyzed the data, and edited the manuscript. GH designed the experiments and wrote and edited the manuscript.

FUNDING

This work was funded by a grant from the Department of Biotechnology, Ministry of Science and Technology, Govt. of India (BT/PR6371/COE/34/19/2013) and core funds from National Centre for Biological Sciences (NCBS), TIFR, to GH. RG is funded by a Post-doctoral fellowship from the Department of Biotechnology, Govt. of India.

ACKNOWLEDGMENTS

We are grateful to Central Imaging and Flow Cytometry Facility, Stem Cell Facility, NCBS, TIFR for use of microscopes and thank Preethi Ravi for help with confocal microscopy. We also thank the NGS facility at NCBS for help with making RNA-Seq cDNA libraries.

SUPPLEMENTARY MATERIAL

The Supplementary Material for this article can be found online at: <https://www.frontiersin.org/articles/10.3389/fnmol.2018.00178/full#supplementary-material>

FIGURE S1 | Experimental design. (1) Small molecule-derived neural precursor cells (NPCs) were derived from the human embryonic stem cell line (hESC) H9 using a dual smad inhibition protocol with small molecules. (2) NPCs were transduced with *STIM1* shRNA-miR to generate a stable knockdown line. (3) *STIM1* knockdown was validated with Ca^{2+} imaging to confirm the attenuation of store-operated Ca^{2+} entry (SOCE) and western blot for validation of a corresponding decrease in *STIM1* protein levels. (4) RNA-Seq analysis was performed to understand the global transcriptional changes subsequent to *STIM1* knockdown in the control NTC and *STIM1* knockdown NPCs. (5) Data analysis after RNA-Seq led to enriched biological pathways which are significantly up/downregulated in the *STIM1* knockdown NPCs. The differentially expressed genes (DEGs) and pathways were taken as cues to conduct proliferation assays (phenotype) and other readouts to corroborate the bioinformatic analyses to the

observed morphological changes. The findings were validated at the protein level by immunostaining and western blots. hESC, human embryonic stem cells; hNPCs, human small molecule-derived neural precursor cells; *STIM1* KD hNPCs, *STIM1* knockdown human small molecule-derived neural precursor cells; NTC, non-targeting control (vector control); DEGs, differentially expressed genes.

FIGURE S2 | Cell growth assays. (A) Growth curve of the control NTC and *STIM1* knockdown NPCs grown as adherent monolayer at 5 DIV in triplicates, $n = 3$. (B) MTT assay showing significant decrease in cell growth in the *STIM1* knockdown NPCs when normalized to the NTC control cells, $n = 5$, $p = 0.008$. DMSO was used to solubilize formazan crystals. MTT assay was performed during the log phase of the cell cycle and cellular metabolic activity due to NAD(P)H flux resulting in formazan production was used as an indicator of viable cells or proliferation. Cells at corresponding phases of cell cycle were stained separately with trypan blue to rule out apoptosis as a reason of low metabolic activity.

FIGURE S3 | Original images of Western blots. NTC, NTC1 and NTC2 represent biological replicates of control NPCs and KD, KD1 and KD2 represent corresponding *STIM1* knockdown NPCs. Molecular weight markers and loading order of lanes in each blot are indicated in each panel. (A) Full blots for **Figures 2D, 6M**. Green box indicates the cropped area shown in **Figure 2D**, red box indicates the cropped area shown in **Figure 6M**. Top panel - *STIM1* (85 kDa), bottom panel - Actin (42 kDa). (B) Red box indicates the cropped area shown in **Figure 6N**. Top panel - Sox2 (35 kDa), bottom panel - Actin. Due to similar molecular weights Sox2 and Actin were run on adjacent lanes in the same gel. (C) Red box indicates the cropped area shown in **Figure 6O**. Left panel - Doublecortin (45 kDa), right panel - Actin. Due to similar molecular weights Doublecortin and Actin were run on adjacent lanes in the same gel. (D) Red box indicates the cropped area shown in **Figure 6P**. Left panel - Tuj1 (55 kDa), right panel - Actin. The same blot is shown at different exposures.

REFERENCES

- Abdullaev, I. F., Bisailon, J. M., Potier, M., Gonzalez, J. C., Motiani, R. K., and Trebak, M. (2008). Stim1 and orail mediate crac currents and store-operated calcium entry important for endothelial cell proliferation. *Circ. Res.* 103, 1289–1299. doi: 10.1161/01.RES.0000338496.95579.56
- Altman, J., and Das, G. D. (1965). Post-natal origin of microneurons in the rat brain. *Nature* 207, 953–956. doi: 10.1038/207953a0
- Anders, S., and Huber, W. (2010). Differential expression analysis for sequence count data. *Genome Biol.* 11:R106. doi: 10.1186/gb-2010-11-10-r106
- Anders, S., Pyl, P. T., and Huber, W. (2015). HTSeq-A Python framework to work with high-throughput sequencing data. *Bioinformatics* 31, 166–169. doi: 10.1093/bioinformatics/btu638
- Arruda, A. P., Pers, B. M., Parlakgul, G., Güney, E., Goh, T., Cagampan, E., et al. (2017). Defective *STIM*-mediated store operated Ca^{2+} entry in hepatocytes leads to metabolic dysfunction in obesity. *eLife* 6:e29968. doi: 10.7554/eLife.29968
- Auyeung, V. C., Ulitsky, I., McGeary, S. E., and Bartel, D. P. (2013). Beyond secondary structure: primary-sequence determinants license PrimiRNA hairpins for processing. *Cell* 152, 844–858. doi: 10.1016/j.cell.2013.01.031
- Bardo, S., Cavazzini, M. G., and Emptage, N. (2006). The role of the endoplasmic reticulum Ca^{2+} store in the plasticity of central neurons. *Trends Pharmacol. Sci.* 27, 78–84. doi: 10.1016/j.tips.2005.12.008
- Baumbach, J., Hummel, P., Bickmeyer, I., Kowalczyk, K. M., Frank, M., Knorr, K., et al. (2014). A *Drosophila* in vivo screen identifies store-operated calcium entry as a key regulator of adiposity. *Cell Metab.* 19, 331–343. doi: 10.1016/j.cmet.2013.12.004
- Béliveau, É., Lessard, V., and Guillemette, G. (2014). *STIM1* positively regulates the Ca^{2+} release activity of the inositol 1,4,5-trisphosphate receptor in bovine aortic endothelial cells. *PLoS One* 9:e114718. doi: 10.1371/journal.pone.0114718
- Bez, A., Corsini, E., Curti, D., Biggiogera, M., Colombo, A., Nicosia, R. F., et al. (2003). Neurosphere and neurosphere-forming cells: morphological and ultrastructural characterization. *Brain Res.* 993, 18–29. doi: 10.1016/j.brainres.2003.08.061
- Boldrini, M., Fulmore, C. A., Tartt, A. N., Simeon, L. R., Pavlova, I., Poposka, V., et al. (2018). Human hippocampal neurogenesis persists throughout aging. *Cell Stem Cell* 22, 589.e5–599.e5. doi: 10.1016/j.stem.2018.03.015
- Bootman, M. D., Collins, T. J., Mackenzie, L., Roderick, H. L., Berridge, M. J., and Peppiatt, C. M. (2002). 2-aminoethoxydiphenyl borate (2-APB) is a reliable blocker of store-operated Ca^{2+} entry but an inconsistent inhibitor of *InsP3*-induced Ca^{2+} release. *FASEB J.* 16, 1145–1150. doi: 10.1096/fj.02-0037rev
- Brafman, D. A. (2015). Generation, expansion, and differentiation of human pluripotent stem cell (hPSC) derived neural progenitor cells (NPCs). *Methods Mol. Biol.* 1212, 87–102. doi: 10.1007/7651_2014_90
- Brandman, O., Liou, J., Park, W. S., and Meyer, T. (2007). *STIM2* is a feedback regulator that stabilizes basal cytosolic and endoplasmic reticulum Ca^{2+} levels. *Cell* 131, 1327–1339. doi: 10.1016/j.cell.2007.11.039
- Burke, L. P., and Kukoly, C. A. (2008). Statins induce lethal effects in acute myeloblastic lymphoma cells within 72 hours. *Leuk. Lymphoma* 49, 322–330. doi: 10.1080/10428190701760011
- Cabernard, C., and Doe, C. Q. (2009). Apical/basal spindle orientation is required for neuroblast homeostasis and neuronal differentiation in *Drosophila*. *Dev. Cell* 17, 134–141. doi: 10.1016/j.devcel.2009.06.009
- Cavallucci, V., Fidaleo, M., and Pani, G. (2016). Neural stem cells and nutrients: poised between quiescence and exhaustion. *Trends Endocrinol. Metab.* 27, 756–769. doi: 10.1016/j.tem.2016.06.007
- Chakraborty, S., and Hasan, G. (2017). Spontaneous Ca^{2+} influx in *Drosophila* pupal neurons is modulated by *IP3*-receptor function and influences maturation of the flight circuit. *Front. Mol. Neurosci.* 10:111. doi: 10.3389/fnmol.2017.00111
- Chambers, S. M., Qi, Y., Mica, Y., Lee, G., Zhang, X. J., Niu, L., et al. (2012). Combined small-molecule inhibition accelerates developmental timing and converts human pluripotent stem cells into nociceptors. *Nat. Biotechnol.* 30, 715–720. doi: 10.1038/nbt.2249

- Cramer, S. C., Sur, M., Dobkin, B. H., O'Brien, C., Sanger, T. D., Trojanowski, J. Q., et al. (2011). Harnessing neuroplasticity for clinical applications. *Brain* 134, 1591–1609. doi: 10.1093/brain/awr039
- Cross-Disorder Group of the Psychiatric Genomics Consortium (2013). Identification of risk loci with shared effects on five major psychiatric disorders: a genome-wide analysis. *Lancet* 381, 1371–1379. doi: 10.1016/S0140-6736(12)62129-1
- Culbreth, M. E., Harrill, J. A., Freudenrich, T. M., Mundy, W. R., and Shafer, T. J. (2012). Comparison of chemical-induced changes in proliferation and apoptosis in human and mouse neuroprogenitor cells. *Neurotoxicology* 33, 1499–1510. doi: 10.1016/j.neuro.2012.05.012
- Deng, W., Wang, Y., Liu, Z., Cheng, H., and Xue, Y. (2014). HemI: a toolkit for illustrating heatmaps. *PLoS One* 9:e111988. doi: 10.1371/journal.pone.0111988
- Dennis, G., Sherman, B. T., Hosack, D. A., Yang, J., Gao, W., Lane, H., et al. (2003). DAVID: database for annotation, visualization, and integrated discovery. *Genome Biol.* 4:R60. doi: 10.1186/gb-2003-4-9-r60
- Di Lullo, E., and Kriegstein, A. R. (2017). The use of brain organoids to investigate neural development and disease. *Nat. Rev. Neurosci.* 18, 573–584. doi: 10.1038/nrn.2017.107
- Domenichini, F., Terrié, E., Arnault, P., Harnois, T., Magaud, C., Bois, P., et al. (2018). Store-operated calcium entries control neural stem cell self-renewal in the adult brain subventricular zone. *Stem Cells* 36, 761–774. doi: 10.1002/stem.2786
- Edgar, R., Domrachev, M., and Lash, A. E. (2002). Gene expression omnibus: NCBI gene expression and hybridization array data repository. *Nucleic Acids Res.* 30, 207–210.
- Efe, J. A., and Ding, S. (2011). The evolving biology of small molecules: controlling cell fate and identity. *Philos. Trans. R. Soc. B Biol. Sci.* 366, 2208–2221. doi: 10.1098/rstb.2011.0006
- egger, B., Gold, K. S., and Brand, A. H. (2010). Notch regulates the switch from symmetric to asymmetric neural stem cell division in the *Drosophila* optic lobe. *Development* 137, 2981–2987. doi: 10.1242/dev.051250
- Elder, G. A., De Gasperi, R., and Gama Sosa, M. A. (2006). Research update: neurogenesis in adult brain and neuropsychiatric disorders. *Mt. Sinai J. Med.* 73, 931–940.
- Elkabetz, Y., Panagiotakos, G., Al Shamy, G., Socci, N. D., Tabar, V., and Studer, L. (2008). Human ES cell-derived neural rosettes reveal a functionally distinct early neural stem cell stage. *Genes Dev.* 22, 152–165. doi: 10.1101/gad.1616208
- Favaro, R., Valotta, M., Ferri, A. L. M., Latorre, E., Mariani, J., Giachino, C., et al. (2009). Hippocampal development and neural stem cell maintenance require Sox2-dependent regulation of Shh. *Nat. Neurosci.* 12, 1248–1256. doi: 10.1038/nn.2397
- Feng, W., and Zhang, M. (2009). Organization and dynamics of PDZ-domain-related supramodules in the postsynaptic density. *Nat. Rev. Neurosci.* 10, 87–99. doi: 10.1038/nrn2540
- Feske, S., Giltman, J., Dolmetsch, R., Staudt, L. M., and Rao, A. (2001). Gene regulation mediated by calcium signals in T lymphocytes. *Nat. Immunol.* 2, 316–324. doi: 10.1038/86318
- Feske, S., Gwack, Y., Prakriya, M., Srikanth, S., Puppel, S. H., Tanasa, B., et al. (2006). A mutation in Orail causes immune deficiency by abrogating CRAC channel function. *Nature* 441, 179–185. doi: 10.1038/nature04702
- Feske, S., Prakriya, M., Rao, A., and Lewis, R. S. (2005). A severe defect in CRAC Ca²⁺ channel activation and altered K⁺ channel gating in T cells from immunodeficient patients. *J. Exp. Med.* 202, 651–662. doi: 10.1084/jem.20050687
- Florio, M., and Huttner, W. B. (2014). Neural progenitors, neurogenesis and the evolution of the neocortex. *Development* 141, 2182–2194. doi: 10.1242/dev.090571
- Forstyuk, O., Romanyuk, N., Verkhatsky, A., Sykova, E., and Dayanithi, G. (2013). Plasticity of calcium signaling cascades in human embryonic stem cell-derived neural precursors. *Stem Cells Dev.* 22, 1506–1521. doi: 10.1089/scd.2012.0624
- Francis, F., Koulakoff, A., Boucher, D., Chafey, P., Schaar, B., Vinet, M. C., et al. (1999). Doublecortin is a developmentally regulated, microtubule-associated protein expressed in migrating and differentiating neurons. *Neuron* 23, 247–256. doi: 10.1016/S0896-6273(00)80777-1
- Gage, F. (2000). Mammalian neural stem cells. *Science* 287, 1433–1438. doi: 10.1126/science.287.5457.1433
- Gauthier-Fisher, A., Lin, D. C., Greeve, M., Kaplan, D. R., Rottapel, R., and Miller, F. D. (2009). Lfc and Tctex-1 regulate the genesis of neurons from cortical precursor cells. *Nat. Neurosci.* 12, 735–744. doi: 10.1038/nn.2339
- Goff, L. A., Trapnell, C., and Kelley, D. (2012). *CummeRbund: Visualization and Exploration of Cufflinks High-Throughput Sequencing Data. R Package Version 22.*
- Grynkiewicz, G., Poenie, M., and Tsien, R. Y. (1985). A new generation of Ca²⁺ indicators with greatly improved fluorescence properties. *J. Biol. Chem.* 260, 3440–3450.
- Guemez-Gamboa, A., Xu, L., Meng, D., and Spitzer, N. C. (2014). Non-cell-autonomous mechanism of activity-dependent neurotransmitter switching. *Neuron* 82, 1004–1016. doi: 10.1016/j.neuron.2014.04.029
- Gwack, Y., Feske, S., Srikanth, S., Hogan, P. G., and Rao, A. (2007). Signalling to transcription: store-operated Ca²⁺ entry and NFAT activation in lymphocytes. *Cell Calcium* 42, 145–156. doi: 10.1016/j.ceca.2007.03.007
- Harrill, J. A., Freudenrich, T. M., Robinette, B. L., and Mundy, W. R. (2011). Comparative sensitivity of human and rat neural cultures to chemical-induced inhibition of neurite outgrowth. *Toxicol. Appl. Pharmacol.* 256, 268–280. doi: 10.1016/j.taap.2011.02.013
- Harris, E., Burki, U., Marini-Bettolo, C., Neri, M., Scotton, C., Hudson, J., et al. (2017). Complex phenotypes associated with STIM1 mutations in both coiled coil and EF-hand domains. *Neuromuscul. Disord.* 27, 861–872. doi: 10.1016/j.nmd.2017.05.002
- Hartmann, J., Karl, R. M., Alexander, R. P. D., Adelsberger, H., Brill, M. S., Rühlmann, C., et al. (2014). STIM1 controls neuronal Ca²⁺ signaling, mGluR1-dependent synaptic transmission, and cerebellar motor behavior. *Neuron* 82, 635–644. doi: 10.1016/j.neuron.2014.03.027
- Homem, C. C. F., Repic, M., and Knoblich, J. A. (2015). Proliferation control in neural stem and progenitor cells. *Nat. Rev. Neurosci.* 16, 647–659. doi: 10.1038/nrn4021
- Homem, C. C. F., Steinmann, V., Burkard, T. R., Jais, A., Esterbauer, H., and Knoblich, J. A. (2014). Ecdysone and mediator change energy metabolism to terminate proliferation in *Drosophila* neural stem cells. *Cell* 158, 874–888. doi: 10.1016/j.cell.2014.06.024
- Huttner, W. B., and Kosodo, Y. (2005). Symmetric versus asymmetric cell division during neurogenesis in the developing vertebrate central nervous system. *Curr. Opin. Cell Biol.* 17, 648–657. doi: 10.1016/j.ceb.2005.10.005
- Ince-Dunn, G., Okano, H. J., Jensen, K. B., Park, W. Y., Zhong, R., Ule, J., et al. (2012). Neuronal Elav-like (Hu) proteins regulate RNA splicing and abundance to control glutamate levels and neuronal excitability. *Neuron* 75, 1067–1079. doi: 10.1016/j.neuron.2012.07.009
- Ishibashi, M., Ang, S. L., Shiota, K., Nakanishi, S., Kageyama, R., and Guillemot, F. (1995). Targeted disruption of mammalian hairy and Enhancer of split homolog-1 (HES-1) leads to up-regulation of neural helix-loop-helix factors, premature neurogenesis, and severe neural tube defects. *Genes Dev.* 9, 3136–3148. doi: 10.1101/gad.9.24.3136
- Jairaman, A., and Prakriya, M. (2013). Molecular pharmacology of store-operated CRAC channels. *Channels* 7, 402–414. doi: 10.4161/chan.25292
- Karsten, S. L., Kudo, L. C., Jackson, R., Sabatti, C., Kornblum, H. I., and Geschwind, D. H. (2003). Global analysis of gene expression in neural progenitors reveals specific cell-cycle, signaling, and metabolic networks. *Dev. Biol.* 261, 165–182. doi: 10.1016/S0012-1606(03)00274-4
- Kawamoto, E. M., Vivar, C., and Camandola, S. (2012). Physiology and pathology of calcium signaling in the brain. *Front. Pharmacol.* 3:61. doi: 10.3389/fphar.2012.00061
- Kennedy, T. E., Serafini, T., de la Torre, J. R., and Tessier-Lavigne, M. (1994). Netrins are diffusible chemotropic factors for commissural axons in the embryonic spinal cord. *Cell* 78, 425–435. doi: 10.1016/0092-8674(94)90421-9
- Kim, D., Langmead, B., and Salzberg, S. L. (2015). HISAT: a fast spliced aligner with low memory requirements. *Nat. Methods* 12, 357–360. doi: 10.1038/nmeth.3317
- Kim, D. Y., Rhee, I., and Paik, J. (2014). Metabolic circuits in neural stem cells. *Cell Mol. Life Sci.* 71, 4221–4241. doi: 10.1007/s00018-014-1686-0
- Klassen, H., Schwartz, M. R., Bailey, A. H., and Young, M. J. (2001). Surface markers expressed by multipotent human and mouse neural progenitor cells

- include tetraspanins and non-protein epitopes. *Neurosci. Lett.* 312, 180–182. doi: 10.1016/S0304-3940(01)02215-7
- Knobloch, M., Braun, S. M. G., Zurkirchen, L., Von Schoultz, C., Zamboni, N., Araújo-Bravo, M. J., et al. (2013). Metabolic control of adult neural stem cell activity by Fasn-dependent lipogenesis. *Nature* 493, 226–230. doi: 10.1038/nature11689
- Knobloch, R., Singec, I., Ditter, M., Pantazis, G., Capetian, P., Meyer, R. P., et al. (2010). Murine features of neurogenesis in the human hippocampus across the lifespan from 0 to 100 years. *PLoS One* 5:e8809. doi: 10.1371/journal.pone.0008809
- Knott, S. R. V., Maceli, A. R., Erard, N., Chang, K., Marran, K., Zhou, X., et al. (2014). A computational algorithm to predict shRNA potency. *Mol. Cell* 56, 796–807. doi: 10.1016/j.molcel.2014.10.025
- Korkotian, E., Oni-Biton, E., and Segal, M. (2017). The role of the store-operated calcium entry channel Orail1 in cultured rat hippocampal synapse formation and plasticity. *J. Physiol.* 595, 125–140. doi: 10.1113/JP272645
- Ladran, I., Tran, N., Topol, A., and Brennand, K. J. (2013). Neural stem and progenitor cells in health and disease. *Wiley Interdiscip. Rev. Syst. Biol. Med.* 5, 701–715. doi: 10.1002/wsbm.1239
- Lalonde, J., Saia, G., and Gill, G. (2014). Store-operated calcium entry promotes the degradation of the transcription factor Sp4 in resting neurons. *Sci. Signal.* 7:ra51. doi: 10.1126/scisignal.2005242
- Lazzari, C., Peggion, C., Stella, R., Massimino, M. L., Lim, D., Bertoli, A., et al. (2011). Cellular prion protein is implicated in the regulation of local Ca²⁺ movements in cerebellar granule neurons. *J. Neurochem.* 116, 881–890. doi: 10.1111/j.1471-4159.2010.07015.x
- Leclerc, C., Daguzan, C., Nicolas, M. T., Chabret, C., Duprat, A. M., and Moreau, M. (1997). L-type calcium channel activation controls the in vivo transduction of the neuralizing signal in the amphibian embryos. *Mech. Dev.* 64, 105–110. doi: 10.1016/S0925-4773(97)00054-3
- Leclerc, C., Néant, I., and Moreau, M. (2012). The calcium: an early signal that initiates the formation of the nervous system during embryogenesis. *Front. Mol. Neurosci.* 5:3. doi: 10.3389/fnfmol.2012.00064
- Leclerc, C., Webb, S. E., Daguzan, C., Moreau, M., and Miller, A. L. (2000). Imaging patterns of calcium transients during neural induction in *Xenopus laevis* embryos. *J. Cell Sci.* 113, 3519–3529.
- Leissring, M. A., Akbari, Y., Fanger, C. M., Cahalan, M. D., Mattson, M. P., and LaFerla, F. M. (2000). Capacitative calcium entry deficits and elevated luminal calcium content in mutant presenilin-1 knockin mice. *J. Cell Biol.* 149, 793–797. doi: 10.1083/jcb.149.4.793
- Lewis, R. S. (2007). The molecular choreography of a store-operated calcium channel. *Nature* 446, 284–287. doi: 10.1038/nature05637
- Lewis, R. S. (2011). Store-operated calcium channels: new perspectives on mechanism and function. *Cold Spring Harb. Perspect. Biol.* 3:a003970. doi: 10.1101/cshperspect.a003970
- Li, H., Handsaker, B., Wysoker, A., Fennell, T., Ruan, J., Homer, N., et al. (2009). The sequence alignment/map format and SAMtools. *Bioinformatics* 25, 2078–2079. doi: 10.1093/bioinformatics/btp352
- Li, W., Sun, W., Zhang, Y., Wei, W., Ambasadhan, R., Xia, P., et al. (2011). Rapid induction and long-term self-renewal of primitive neural precursors from human embryonic stem cells by small molecule inhibitors. *Proc. Natl. Acad. Sci. U.S.A.* 108, 8299–8304. doi: 10.1073/pnas.1014041108
- Lin, Y., Golovkina, K., Chen, Z.-X., Lee, H. N., Negron, Y. L. S., Sultana, H., et al. (2016). Comparison of normalization and differential expression analyses using RNA-Seq data from 726 individual *Drosophila melanogaster*. *BMC Genomics* 17:28. doi: 10.1186/s12864-015-2353-z
- Liou, J., Kim, M. L., Won, D. H., Jones, J. T., Myers, J. W., Ferrell, J. E., et al. (2005). STIM is a Ca²⁺ sensor essential for Ca²⁺-store-depletion-triggered Ca²⁺ influx. *Curr. Biol.* 15, 1235–1241. doi: 10.1016/j.cub.2005.05.055
- Louis, L. K., Gopurappilly, R., Surendran, H., Dutta, S., and Pal, R. (2017). Transcriptional profiling of human neural precursors post alcohol exposure reveals impaired neurogenesis via dysregulation of ERK signaling and miR-145. *J. Neurochem.* doi: 10.1111/jnc.14155 [Epub ahead of print].
- Lytton, J., Westlin, M., and Hanley, M. R. (1991). Thapsigargin inhibits the sarcoplasmic or endoplasmic reticulum Ca-ATPase family of calcium pumps. *J. Biol. Chem.* 266, 17067–17071.
- Majewski, L., and Kuznicki, J. (2015). SOCE in neurons: signaling or just refilling? *Biochim. Biophys. Acta* 1853, 1940–1952. doi: 10.1016/j.bbamcr.2015.01.019
- Malmersjö, S., Liste, I., Dyachok, O., Tengholm, A., Arenas, E., and Uhlén, P. (2010). Ca²⁺ and cAMP signaling in human embryonic stem cell-derived dopamine neurons. *Stem Cells Dev.* 19, 1355–1364. doi: 10.1089/scd.2009.0436
- Mao, X., Yang, S. H., Simpkins, J. W., and Barger, S. W. (2007). Glutamate receptor activation evokes calpain-mediated degradation of Sp3 and Sp4, the prominent Sp-family transcription factors in neurons. *J. Neurochem.* 100, 1300–1314. doi: 10.1111/j.1471-4159.2006.04297.x
- Marek, K. W., Kurtz, L. M., and Spitzer, N. C. (2010). cJun integrates calcium activity and tlx3 expression to regulate neurotransmitter specification. *Nat. Neurosci.* 13, 944–950. doi: 10.1038/nn.2582
- Maus, M., Cuk, M., Patel, B., Lian, J., Ouimet, M., Kaufmann, U., et al. (2017). Store-Operated Ca²⁺ entry controls induction of lipolysis and the transcriptional reprogramming to lipid metabolism. *Cell Metab.* 25, 698–712. doi: 10.1016/j.cmet.2016.12.021
- McNally, B. A., and Prakriya, M. (2012). Permeation, selectivity and gating in store-operated CRAC channels. *J. Physiol.* 590, 4179–4191. doi: 10.1113/jphysiol.2012.233098
- Muller, M. S., Fox, R., Schousboe, A., Waagepetersen, H. S., and Bak, L. K. (2014). Astrocyte glycogenolysis is triggered by store-operated calcium entry and provides metabolic energy for cellular calcium homeostasis. *Glia* 62, 526–534. doi: 10.1002/glia.22623
- Neely, M. D., Litt, M. J., Tidball, A. M., Li, G. G., Aboud, A. A., Hopkins, C. R., et al. (2012). DMH1, a highly selective small molecule BMP inhibitor promotes neurogenesis of hiPSCs: comparison of PAX6 and SOX1 expression during neural induction. *ACS Chem. Neurosci.* 3, 482–491. doi: 10.1021/cn300029t
- Nekrasov, E. D., Vigont, V. A., Klyushnikov, S. A., Lebedeva, O. S., Vassina, E. M., Bogomazova, A. N., et al. (2016). Manifestation of Huntington's disease pathology in human induced pluripotent stem cell-derived neurons. *Mol. Neurodegener.* 11:27. doi: 10.1186/s13024-016-0092-5
- Ohga, K., Takezawa, R., Arakida, Y., Shimizu, Y., and Ishikawa, J. (2008). Characterization of YM-58483/BTP2, a novel store-operated Ca²⁺ entry blocker, on T cell-mediated immune responses in vivo. *Int. Immunopharmacol.* 8, 1787–1792. doi: 10.1016/j.intimp.2008.08.016
- Ostenfeld, T., Caldwell, M. A., Prowse, K. R., Linskens, M. H., Jauniaux, E., and Svendsen, C. N. (2000). Human neural precursor cells express low levels of telomerase in vitro and show diminishing cell proliferation with extensive axonal outgrowth following transplantation. *Exp. Neurol.* 164, 215–226. doi: 10.1006/exnr.2000.7427
- Ostenfeld, T., Joly, E., Tai, Y. T., Peters, A., Caldwell, M., Jauniaux, E., et al. (2002). Regional specification of rodent and human neurospheres. *Dev. Brain Res.* 134, 43–55. doi: 10.1016/S0165-3806(01)00291-7
- Pacey, L., Stead, S., Gleave, J., Tomczyk, K., and Doering, L. C. (2006). Neural stem cell culture: neurosphere generation, microscopical analysis and cryopreservation. *Protoc. Exch.* doi: 10.1038/nprot.2006.215
- Pathak, T., Agrawal, T., Richhariya, S., Sadaf, S., and Hasan, G. (2015). Store-operated calcium entry through orai1 is required for transcriptional maturation of the flight circuit in *Drosophila*. *J. Neurosci.* 35, 13784–13799. doi: 10.1523/JNEUROSCI.1680-15.2015
- Pathak, T., Trivedi, D., and Hasan, G. (2017). CRISPR-Cas-induced mutants identify a requirement for dSTIM in larval dopaminergic cells of *Drosophila melanogaster*. *G3* 7, 923–933. doi: 10.1534/g3.116.038539
- Pathan, M., Keerthikumar, S., Ang, C. S., Gangoda, L., Quek, C. Y. J., Williamson, N. A., et al. (2015). FunRich: an open access standalone functional enrichment and interaction network analysis tool. *Proteomics* 15, 2597–2601. doi: 10.1002/pmic.201400515
- Pavlidis, P., and Noble, W. S. (2003). Matrix2png: a utility for visualizing matrix data. *Bioinformatics* 19, 295–296. doi: 10.1093/bioinformatics/19.2.295
- Pelzl, L., Hauser, S., Elsir, B., Sukkar, B., Sahu, I., Singh, Y., et al. (2017). Lithium sensitive ORAI1 expression, store operated Ca²⁺ entry and suicidal death of neurons in chorea-acanthocytosis. *Sci. Rep.* 7:6457. doi: 10.1038/s41598-017-06451-1
- Plazas, P. V., Nicol, X., and Spitzer, N. C. (2013). Activity-dependent competition regulates motor neuron axon pathfinding via PlexinA3. *Proc. Natl. Acad. Sci. U.S.A.* 110, 1524–1529. doi: 10.1073/pnas.1213048110
- Potier, M., Gonzalez, J. C., Motiani, R. K., Abdullaev, I. F., Bisailon, J. M., Singer, H. A., et al. (2009). Evidence for STIM1- and Orail1-dependent store-operated calcium influx through ICRCAC in vascular smooth muscle cells: role

- in proliferation and migration. *FASEB J.* 23, 2425–2437. doi: 10.1096/fj.09-131128
- Prakriya, M., Feske, S., Gwack, Y., Srikanth, S., Rao, A., and Hogan, P. G. (2006). Orail1 is an essential pore subunit of the CRAC channel. *Nature* 443, 230–233. doi: 10.1038/nature05122
- Prakriya, M., and Lewis, R. S. (2001). Potentiation and inhibition of Ca^{2+} release-activated Ca^{2+} channels by 2-aminoethyl-diphenyl borate (2-APB) occurs independently of IP 3 receptors. *J. Physiol.* 536, 3–19. doi: 10.1111/j.1469-7793.2001.t01-1-00003.x
- Prakriya, M., and Lewis, R. S. (2015). Store-operated calcium channels. *Physiol. Rev.* 95, 1383–1436. doi: 10.1152/physrev.00020.2014
- Qian, X., Shen, Q., Goderie, S. K., He, W., Capela, A., Davis, A. A., et al. (2000). Timing of CNS cell generation: a programmed sequence of neuron and glial cell production from isolated murine cortical stem cells. *Neuron* 28, 69–80. doi: 10.1016/S0896-6273(00)00086-6
- Rakic, P. (1995). “Corticogenesis in human and nonhuman primates,” in *The Cognitive Neurosciences*, ed. M. Gazzaniga (Cambridge, MA: MIT Press), 127–145.
- Reinhardt, P., Glatza, M., Hemmer, K., Tsytsyura, Y., Thiel, C. S., Höing, S., et al. (2013). Derivation and expansion using only small molecules of human neural progenitors for neurodegenerative disease modeling. *PLoS One* 8:e59252. doi: 10.1371/journal.pone.0059252
- Reynolds, B. A., and Weiss, S. (1992). Generation of neurons and astrocytes from isolated cells of the adult mammalian central nervous system. *Science* 255, 1707–1710. doi: 10.1126/science.1553558
- Richhariya, S., Jayakumar, S., Abruzzi, K., Rosbash, M., and Hasan, G. (2017). A pupal transcriptomic screen identifies Ral as a target of store-operated calcium entry in *Drosophila* neurons. *Sci. Rep.* 7:42586. doi: 10.1038/srep42586
- Robinson, M. D., McCarthy, D. J., and Smyth, G. K. (2010). edgeR: a Bioconductor package for differential expression analysis of digital gene expression data. *Bioinformatics* 26, 139–140. doi: 10.1093/bioinformatics/btp616
- Roos, J., DiGregorio, P. J., Yeromin, A. V., Ohlsen, K., Lioudyno, M., Zhang, S., et al. (2005). STIM1, an essential and conserved component of store-operated Ca^{2+} channel function. *J. Cell Biol.* 169, 435–445. doi: 10.1083/jcb.200502019
- Rosenberg, S. S., and Spitzer, N. C. (2011). Calcium signaling in neuronal development. *Cold Spring Harb. Perspect. Biol.* 3, 1–13. doi: 10.1101/cshperspect.a004259
- Rusanescu, G., Qi, H., Thomas, S. M., Brugge, J. S., and Halegoua, S. (1995). Calcium influx induces neurite growth through a Src-Ras signaling cassette. *Neuron* 15, 1415–1425. doi: 10.1016/0896-6273(95)90019-5
- Sanai, H., Tramontin, A. D., Quiñones-Hinojosa, A., Barbaro, N. M., Gupta, H., Kunwar, S., et al. (2004). Unique astrocyte ribbon in adult human brain contains neural stem cells but lacks chain migration. *Nature* 427, 740–744. doi: 10.1038/nature02301
- Scholzen, T., and Gerdes, J. (2000). The Ki-67 protein: from the known and the unknown. *J. Cell. Physiol.* 182, 311–322. doi: 10.1002/(SICI)1097-4652(200003)182:3<311::AID-JCP1>3.0.CO;2-9
- Scorrano, L., Oakes, S. A., Opferman, J. T., Cheng, E. H., Sorcinelli, M. D., Pozzan, T., et al. (2003). BAX and BAK regulation of endoplasmic reticulum Ca^{2+} : a control Point for apoptosis. *Science* 300, 135–139. doi: 10.1126/science.1081208
- Seyednasrollah, F., Laiho, A., and Elo, L. L. (2015). Comparison of software packages for detecting differential expression in RNA-seq studies. *Brief. Bioinform.* 16, 59–70. doi: 10.1093/bib/bbt086
- Shi, Y., Sun, G., Zhao, C., and Stewart, R. (2008). Neural stem cell self-renewal. *Crit. Rev. Oncol. Hematol.* 65, 43–53. doi: 10.1016/j.critrevonc.2007.06.004
- Somasundaram, A., Shum, A. K., McBride, H. J., Kessler, J. A., Feske, S., Miller, R. J., et al. (2014). Store-operated CRAC channels regulate gene expression and proliferation in neural progenitor cells. *J. Neurosci.* 34, 9107–9123. doi: 10.1523/JNEUROSCI.0263-14.2014
- Sorrells, S. F., Paredes, M. F., Cebrian-Silla, A., Sandoval, K., Qi, D., Kelley, K. W., et al. (2018). Human hippocampal neurogenesis drops sharply in children to undetectable levels in adults. *Nature* 555, 377–381. doi: 10.1038/nature25975
- Spitzer, N. C. (2012). Activity-dependent neurotransmitter respecification. *Nat. Rev. Neurosci.* 13, 94–106. doi: 10.1038/nrn3154
- Stevens, H. E., Smith, K. M., Rash, B. G., and Vaccarino, F. M. (2010). Neural stem cell regulation, fibroblast growth factors, and the developmental origins of neuropsychiatric disorders. *Front. Neurosci.* 4:59. doi: 10.3389/fnins.2010.00059
- Strzalka, W., and Ziemienowicz, A. (2011). Proliferating cell nuclear antigen (PCNA): a key factor in DNA replication and cell cycle regulation. *Ann. Bot.* 107, 1127–1140. doi: 10.1093/aob/mcq243
- Subramanian, M., Metya, S. K., Sadaf, S., Kumar, S., Schwudke, D., and Hasan, G. (2013). Altered lipid homeostasis in *Drosophila* InsP3 receptor mutants leads to obesity and hyperphagia. *Dis. Models Mech.* 6, 734–744. doi: 10.1242/dmm.010017
- Sun, S., Zhang, H., Liu, J., Popugaeva, E., Xu, N. J., Feske, S., et al. (2014). Reduced synaptic STIM2 expression and impaired store-operated calcium entry cause destabilization of mature spines in mutant presenilin mice. *Neuron* 82, 79–93. doi: 10.1016/j.neuron.2014.02.019
- Thillaiappan, N. B., Chavda, A. P., Tovey, S. C., Prole, D. L., and Taylor, C. W. (2017). Ca^{2+} signals initiate at immobile IP3 receptors adjacent to ER-plasma membrane junctions. *Nat. Commun.* 8:1505. doi: 10.1038/s41467-017-01644-8
- Toni, N., Laplagne, D. A., Zhao, C., Lombardi, G., Ribak, C. E., Gage, F. H., et al. (2008). Neurons born in the adult dentate gyrus form functional synapses with target cells. *Nat. Neurosci.* 11, 901–907. doi: 10.1038/nn.2156
- Toth, A. B., Shum, A. K., and Prakriya, M. (2016). Regulation of neurogenesis by calcium signaling. *Cell Calcium* 59, 124–134. doi: 10.1016/j.ceca.2016.02.011
- Trapnell, C., Roberts, A., Goff, L., Pertea, G., Kim, D., Kelley, D. R., et al. (2012). Differential gene and transcript expression analysis of RNA-seq experiments with TopHat and cufflinks. *Nat. Protoc.* 7, 562–578. doi: 10.1038/nprot.2012.016
- Tsai, F. C., Seki, A., Yang, H. W., Hayer, A., Carrasco, S., Malmersjö, S., et al. (2014). A polarized Ca^{2+} , diacylglycerol and STIM1 signalling system regulates directed cell migration. *Nat. Cell Biol.* 16, 133–144. doi: 10.1038/ncb2906
- Vaeth, M., Maus, M., Klein-Hessling, S., Freinkman, E., Yang, J., Eckstein, M., et al. (2017). Store-Operated Ca^{2+} entry controls clonal expansion of T cells through metabolic reprogramming. *Immunity* 47, 664.e9–679.e9. doi: 10.1016/j.immuni.2017.09.003
- van Praag, H., Schinder, A. F., Christie, B. R., Toni, N., Palmer, T. D., and Gage, F. H. (2002). Functional neurogenesis in the adult hippocampus. *Nature* 415, 1030–1034. doi: 10.1038/4151030a
- Venkiteswaran, G., and Hasan, G. (2009). Intracellular Ca^{2+} signaling and store-operated Ca^{2+} entry are required in *Drosophila* neurons for flight. *Proc. Natl. Acad. Sci. U.S.A.* 106, 10326–10331. doi: 10.1073/pnas.0902982106
- Vig, M., Peinelt, C., Beck, A., Koormo, D. L., Rabah, D., Koblan-Huberson, M., et al. (2006). CRACM1 is a plasma membrane protein essential for store-operated Ca^{2+} entry. *Science* 312, 1220–1223. doi: 10.1126/science.1127883
- Wang, C., Liu, F., Liu, Y. Y., Zhao, C. H., You, Y., Wang, L., et al. (2011). Identification and characterization of neuroblasts in the subventricular zone and rostral migratory stream of the adult human brain. *Cell Res.* 21, 1534–1550. doi: 10.1038/cr.2011.83
- Wang, D., and Gao, L. (2005). Proteomic analysis of neural differentiation of mouse embryonic stem cells. *Proteomics* 5, 4414–4426. doi: 10.1002/pmic.200401304
- Wegner, M. (2011). SOX after SOX: SOXession regulates neurogenesis. *Genes Dev.* 25, 2423–2428. doi: 10.1101/gad.181487.111
- Wu, J., Ryskamp, D. A., Liang, X., Egorova, P., Zakharova, O., Hung, G., et al. (2016). Enhanced store-operated calcium entry leads to striatal synaptic loss in a Huntington’s disease mouse model. *J. Neurosci.* 36, 125–141. doi: 10.1523/JNEUROSCI.1038-15.2016
- Wu, J., Shih, H.-P., Vigont, V., Hrdlicka, L., Diggins, L., Singh, C., et al. (2011). Neuronal store-operated calcium entry pathway as a novel therapeutic target for Huntington’s disease treatment. *Chem. Biol.* 18, 777–793. doi: 10.1016/j.chembiol.2011.04.012
- Yang, M., Yang, S.-L., Herrlinger, S., Liang, C., Dzieciatkowska, M., Hansen, K. C., et al. (2015). Lin28 promotes the proliferative capacity of neural progenitor cells in brain development. *Development* 142, 1616–1627. doi: 10.1242/dev.120543
- Yap, M. S., Nathan, K. R., Yeo, Y., Lim, L. W., Poh, C. L., Richards, M., et al. (2015). Neural differentiation of human pluripotent stem cells for nontherapeutic applications: toxicology, pharmacology, and in vitro disease modeling. *Stem Cells Int.* 2015:105172. doi: 10.1155/2015/105172
- Yoo, A. S., Cheng, I., Chung, S., Grenfell, T. Z., Lee, H., Pack-Chung, E., et al. (2000). Presenilin-mediated modulation of capacitative calcium entry. *Neuron* 27, 561–572. doi: 10.1016/S0896-6273(00)00066-0

- Zhang, H., Wu, L., Pchitskaya, E., Zakharova, O., Saito, T., Saido, T., et al. (2015). Neuronal store-operated calcium entry and mushroom spine loss in amyloid precursor protein knock-in mouse model of Alzheimer's disease. *J. Neurosci.* 35, 13275–13286. doi: 10.1523/JNEUROSCI.1034-15.2015
- Zhang, S.-C., Wernig, M., Duncan, I. D., Brüstle, O., and Thomson, J. A. (2001). In vitro differentiation of transplantable neural precursors from human embryonic stem cells. *Nat. Biotechnol.* 19, 1129–1133. doi: 10.1038/nbt1201-1129
- Zhang, S. L., Yeromin, A. V., Zhang, X. H.-F., Yu, Y., Safrina, O., Penna, A., et al. (2006). Genome-wide RNAi screen of Ca^{2+} influx identifies genes that regulate Ca^{2+} release-activated Ca^{2+} channel activity. *Proc. Natl. Acad. Sci. U.S.A.* 103, 9357–9362. doi: 10.1073/pnas.0603161103
- Zhou, Q., Yen, A., Rymarczyk, G., Asai, H., Trengrove, C., Aziz, N., et al. (2016). Impairment of PARK14-dependent Ca^{2+} signalling is a novel determinant of Parkinson's disease. *Nat. Commun.* 7:10332. doi: 10.1038/ncomms10332

Conflict of Interest Statement: RG and GH are involved in the provisional patent application that is in progress entitled “Human neural precursor cells with inducible STIM1 knockdown to model neurodevelopmental and neuropsychiatric diseases with altered intracellular calcium signaling”.

The remaining authors declare that the research was conducted in the absence of any commercial or financial relationships that could be construed as a potential conflict of interest.

Copyright © 2018 Gopurappilly, Deb, Chakraborty and Hasan. This is an open-access article distributed under the terms of the Creative Commons Attribution License (CC BY). The use, distribution or reproduction in other forums is permitted, provided the original author(s) and the copyright owner are credited and that the original publication in this journal is cited, in accordance with accepted academic practice. No use, distribution or reproduction is permitted which does not comply with these terms.